Mon. Not. R. Astron. Soc. **356,** 270–294 (2005) doi:10.1111/j.1365-2966.2004.08452.x

The stellar populations of low-luminosity active galactic nuclei – III. Spatially resolved spectral properties

R. Cid Fernandes,[1]⋆ R. M. González Delgado,[2]⋆ T. Storchi-Bergmann,[3]⋆
L. Pires Martins[4]⋆ and H. Schmitt[5]⋆†
[1]*Depto. de Física – CFM – Universidade Federal de Santa Catarina, C.P. 476, 88040-900, Florianópolis, SC, Brazil*
[2]*Instituto de Astrofísica de Andalucía (CSIC), PO Box 3004, 18080 Granada, Spain*
[3]*Instituto de Física, Universidade Federal do Rio Grande do Sul, C.P. 15001, 91501-970, Porto Alegre, RS, Brazil*
[4]*Space Telescope Institute, 3700 San Martin Drive, Baltimore, MD 21218, USA*
[5]*National Radio Astronomy Observatory, 520 Edgemont Road, Charlottesville, VA22903-2475, USA*

Accepted 2004 September 23. Received 2004 September 15; in original form 2004 June 17

ABSTRACT

In a recently completed survey of the stellar population properties of low-ionization nuclear emission-line regions (LINERs) and LINER/H II transition objects (TOs), we have identified a numerous class of galactic nuclei which stand out because of their conspicuous 10^{8-9} yr populations, traced by high-order Balmer absorption lines and other stellar indices. These objects are called 'young-TOs', because they all have TO-like emission-line ratios. In this paper we extend this previous work, which concentrated on the nuclear properties, by investigating the radial variations of spectral properties in low-luminosity active galactic nuclei (LLAGNs). Our analysis is based on high signal-to-noise ratio (S/N) long-slit spectra in the 3500–5500 Å interval for a sample of 47 galaxies. The data probe distances of typically up to 850 pc from the nucleus with a resolution of ∼100 pc (∼1 arcsec) and S/N ∼ 30. Stellar population gradients are mapped by the radial profiles of absorption-line equivalent widths and continuum colours along the slit. These variations are further analysed by means of a decomposition of each spectrum in terms of template galaxies representative of very young ($\leqslant 10^7$ yr), intermediate age (10^{8-9} yr) and old (10^{10} yr) stellar populations.

This study reveals that young-TOs also differ from old-TOs and old-LINERs in terms of the spatial distributions of their stellar populations and dust. Specifically, our main findings are as follows. (i) Significant stellar population gradients are found almost exclusively in young-TOs. (ii) The intermediate age population of young-TOs, although heavily concentrated in the nucleus, reaches distances of up to a few hundred pc from the nucleus. Nevertheless, the half width at half-maximum of its brightness profile is more typically 100 pc or less. (iii) Objects with predominantly old stellar populations present spatially homogeneous spectra, be they LINERs or TOs. (iv) Young-TOs have much more dust in their central regions than other LLAGNs. (v) The B-band luminosities of the central $\lesssim 1$ Gyr population in young-TOs are within an order of magnitude of $M_B = -15$, implying masses of the order of $\sim 10^7$–10^8 M$_\odot$. This population was 10–100 times more luminous in its formation epoch, at which time young massive stars would have completely outshone any active nucleus, unless the AGN too was brighter in the past.

Key words: galaxies: active – galaxies: nuclei – galaxies: Seyfert – galaxies: statistics – galaxies: stellar content.

1 INTRODUCTION

Low-luminosity active galactic nuclei (LLAGNs) are the most common form of activity in the nearby Universe. Their proximity allows us to sample their properties on linear scales which are not accessible for farther AGN populations such as Seyferts and quasars. At

---

⋆E-mail: cid@astro.ufsc.br (RCF); rosa@iaa.es (RMGD); thaisa@if.ufrgs.br (TS-B); martins@stsci.edu (LPM); hschmitt@nrao.edu (HS)
†Jansky Fellow.

optical–ultraviolet wavelengths, however, this advantage is compensated by the difficulty in isolating the light from these intrinsically weak nuclei out of a dominant stellar 'background'.

In a series of papers, we have been working on our own contribution to this field. In Cid Fernandes et al. (2004a, hereafter Paper I) we analysed ground-based nuclear optical spectra of a sample of 51 low-ionization nuclear emission-line regions (LINERs) and transition objects (TOs), while in González Delgado et al. (2004, hereafter Paper II) we complement this data set with archive *Hubble Space Telescope* (*HST*) Space Telescope Imaging Spectrograph (STIS) spectra of 28 nearby LLAGNs. These samples cover nearly half of the LLAGNs in the survey of Ho, Filippenko & Sargent (1997, hereafter HFS97). Our focus throughout this series is on the stellar populations of LLAGNs, with the ultimate goal of establishing the role of stellar processes in the physics of these objects.

The main result of Papers I and II is that we have uncovered a very strong relation between the nuclear stellar population and the gas excitation, as measured by [O I]/Hα, the most important diagnostic line ratio in LLAGNs. The relation is in the sense that virtually all systems containing strong populations of ∼1 Gyr or less have [O I]/H$\alpha \leqslant 0.25$, while nuclei dominated by older stars span the full range in [O I]/Hα (up to nearly 1). In other words, virtually all systems with relatively young stellar populations have TO-like emission-line spectra, whereas older nuclei can have either TO- or LINER-like line ratios. This finding led us to introduce a combined stellar population and emission-line classification in four types: young-TOs, old-TOs, old-LINERs and young-LINERs. This latter class is extremely rare.

This relation between line ratios and stellar population is analogous to that found in Seyfert 2s, where nuclei with strong circumnuclear starbursts tend to have relatively small values of [O III]/Hβ and He II/Hβ, while systems dominated by old stars can reach larger values of these line ratios (Cid Fernandes et al. 2001 and references therein). It is thus tempting to interpret young-TOs as low-luminosity analogues of starburst plus Seyfert 2 composites, where the relatively low excitation is explained by the starburst contribution to Hβ, which dilutes [O III]/Hβ and He II/Hβ. Intriguingly, however, young-TOs are substantially older than the starbursts around Seyfert 2 nuclei, many of which are just a few Myr old, as deduced by the detection of O and WR stars. While Papers I and II have revealed a surprisingly large number of systems containing 10^8–10^9 yr populations, massive young stars of the type often found in Seyfert 2s seem to be rare in LLAGNs. The analogy between young-TOs and starburst plus Seyfert 2 composites thus rests upon the hypothesis of the existence of a population of massive stars which remains essentially undetected at optical wavelengths. Clearly, further work is necessary to clarify the precise nature of the connection between stellar and gaseous properties in LLAGNs.

One type of study which has been carried out for Seyferts is the mapping of stellar populations based on spatially resolved spectroscopy. Variations of absorption-line equivalent widths (W_λ) and colours (C_λ) as a function of distance from the nucleus were mapped by means of long-slit spectroscopy by Cid Fernandes, Storchi-Bergmann & Schmitt (1998), Boisson et al. (2000), González Delgado, Heckman & Leitherer (2001) and Joguet et al. (2001). These variations can be transformed into stellar population profiles, as in the study by Raimann et al. (2003), who found that star formation in starburst plus Seyfert 2s composites, although concentrated in the central regions, is not confined to the nucleus, but spread over the inner ∼1 kpc. Spatial gradients in spectral indices are also useful to detect the presence of a central continuum source, which dilutes the nuclear W_λ with respect to off-nuclear positions. Both a compact nuclear starburst and an AGN featureless continuum can produce this effect, but in Seyfert 2s the papers above have shown that significant dilution only occurs when a starburst is present in the innermost extraction.

Spatially resolved spectroscopy of LLAGNs has so far been limited to relatively few studies (e.g. Cid Fernandes et al. 1998). While these previous works advanced our comprehension of individual sources, the small number of objects, differences in spectral coverage, data quality and method of analysis prevents us from drawing general conclusions about the radial distribution of stellar populations in LINERs and TOs. In this third paper we take advantage of our recently completed spectroscopic survey to extend this type of study to a large sample of LLAGNs. Variations of spectral properties with distance from the nucleus are mapped with the general goal of investigating the relation between spatial gradients, emission-line and nuclear stellar population properties. In particular, we aim at evaluating the spatial distribution of intermediate age populations, a distinguishing feature of young-TOs.

In Section 2 we describe the data set and present examples of our spatially resolved spectra. In Section 3 we investigate the spatial variations of a set of spectral properties and quantify these gradients by means of suitable empirical indices. These gradients are further analysed in Section 4 with the goal of producing estimates of the sizes, luminosities, masses and extinction of the intermediate stellar population in the central regions of young-TOs. These estimates provide useful hints on the past and future history of these sources. Finally, in Section 5 we summarize our results.

2 DATA

The data employed in this paper have been described in Paper I. Briefly, we have collected long-slit spectra in the 3500–5500 Å range for 60 galaxies selected out of the HFS97 survey. Observations were carried out at the 2.5-m Nordic Optical Telescope (NOT) with a 1-arcsec slit-width and the Kitt Peak National Observatory (KPNO) 2.1-m telescope with a 2-arcsec slit. Our survey differs from that of our mother sample in two main aspects: wavelength coverage and spatial resolution. The information encoded in the region bluewards of 4200 Å, not covered by HFS97, has been explored in previous papers in this series. Here we concentrate on the analysis of the spatial information in this data set.

2.1 Extractions

In order to map spectral gradients, spectra were extracted in several positions along the slit. Extractions for the KPNO spectra were made at every 2.34 arcsec (3 pixel) out to at least $\theta = \pm 4.7$ arcsec, but the seeing was 2–3 arcsec (FWHM). For the NOT spectra, which constitute 83 per cent of the data analysed here, we have used 1.13 arcsec (6 pixel) long extractions out to at least $\theta = 4.5$ arcsec from the nucleus in both directions. These narrow extractions approximately match the angular resolution of our typical NOT observations, which were made under subarcsec seeing. Outside this central region, wider extractions were used if necessary to ensure enough signal.

The signal-to-noise (S/N) ratio in each extraction was estimated from the rms fluctuation in the 4789–4839 Å interval. Galaxies with $(S/N)_{\lambda 4800} \lesssim 15$ at angular distances $\leqslant 4.7$ arcsec from the nucleus were deemed to have insufficient useful spatial coverage and discarded from the analysis. Our cleaned sample contains 47 objects, including four normal galaxies and one starburst nucleus. In the nuclear extractions $(S/N)_{\lambda 4800}$ varies between 31 and 88 with a median of 51. Outside the nucleus, the median $(S/N)_{\lambda 4800}$ decreases from 45 at $\theta = \pm 2.3$ arcsec to 31 at $\pm$ 4.5 arcsec. The S/N in the 4010–4060 Å interval is typically 0.5 $(S/N)_{\lambda 4800}$. All 521 extractions were dereddened by Galactic extinction using the Cardelli, Clayton & Mathis (1989) law and the A_B values of Schlegel, Finkbeiner & Davis (1998). We note that the KPNO observations (seven galaxies) were taken under non-photometric conditions. This however affects only the absolute flux scale, not the shape of the spectrum, as we verified by comparing spectra of objects taken on both photometric and non-photometric nights. The single result reported in this paper which is affected by this problem is the luminosity of the central young population in NGC 404 (Section 4.2.3), which is likely underestimated.

The distances to the LLAGNs in this sample vary between $d =$ 2.4 and 70.6 Mpc, with a median of 24.1 Mpc. At these distances, $\theta = 4.5$ arcsec corresponds to projected radii $r = 52$–1540 pc, with a median of 526 pc, while our nuclear extractions correspond to 11–204 pc in radius (median = 85 pc). The spatial regions sampled by these observations are therefore smaller than those in our studies of Seyfert 2s (e.g. Raimann et al. 2003), which sampled the inner few kpc with a resolution of ~300 pc.

2.2 Sample properties

Table 1 lists our sample, along with the useful spatial coverage in both angular ($\theta_{\rm out}$) and linear ($r_{\rm out}$) units, nuclear and off-nuclear S/N, linear scale, position angle and a summary of spectral properties.

The emission-line classification from HFS97 is listed in column 8 of Table 1. As in Papers I and II, we prefer to classify LLAGNs as either strong or weak [O I] emitters (column 11), with a dividing line at [O I]/Hα = 0.25. These two classes differ only slightly from the LINER and TO classes of HFS97, and better represent the combined distributions of emission-line and stellar population properties of LLAGNs. Throughout this paper, LINERs and TOs are used as synonyms of strong and weak [O I] sources, respectively.

Paper I introduced a stellar population characterization scheme defined in terms of four classes: η = Y, I, I/O and O (column 9). The Y class denotes objects with a dominant young starburst. The only object in our sample which fits this class is the Wolf–Rayet (WR) galaxy NGC 3367, which is not a LLAGN but is kept in the analysis for comparison purposes. Nuclei with strong intermediate age (10^8–10^9 yr) populations, easily identified by high-order Balmer absorption lines (HOBLs; H8λ 3889 and higher) and diluted metal lines, are classed as η = I, while nuclei dominated by old stars are attributed an η = O class, and η = I/O denotes intermediate cases. Not surprisingly, it is sometimes hard to decide where to fit a galaxy in this classification scheme. The best example of this sort of problem is NGC 772, which contains both young, intermediate age and old components (Paper I). Despite the weak HOBLs in its spectrum, we chose to tag it as η = I.

A simpler (but still useful) classification scheme is to group η = Y and I objects as 'young' and η = I/O and O objects as 'old'. As an objective criterion for this classification we use the value of the equivalent width of the Ca II K line in the nucleus: $W_{\rm K}^{\rm nuc} \leqslant 15$ Å for young systems and larger for old ones (column 10). The use of this equivalent width as an indicator of the evolutionary status of the stellar population is justified because the AGN contribution to the continuum is these sources negligible (Papers I and II). These two classes are paired with the [O I]/Hα class to produce our combined stellar population and emission-line classification into young/old-TO/LINER, listed in the last column of Table 1.

Of the 42 LLAGNs in our sample, 13 fit our definition of strong [O I] sources and 29 are weak [O I] sources, while the stellar populations types are split into 16 young and 28 old systems. The combined emission-line and stellar population statistics are: 14 young-TOs, two young-LINERs, 11 old-LINERs and 15 old-TOs. Note that young-LINER is a practically non-existent category, as the overwhelming majority of young systems are weak [O I] emitters.

It is worth pointing out that young-TOs in this sample are, on average, closer than other LLAGNs. The distances to young-TOs span the d = 2.4–35.6 Mpc range, with a median of 16.8 Mpc, while for other LLAGNs $14.3 \leqslant d \leqslant 70.6$ Mpc, with a median of 31.6 Mpc. This tendency is already present in Paper I and in the HFS97 survey, from which we culled our sample. In principle, it is expected that radial variations of spectral properties due to the presence of a compact central source will be harder to detect for more distant objects, due to the increasing contribution of bulge light to the nuclear extraction. This potential difficulty, coupled with the trend discussed above, may lead to a bias in the sense that radial gradients would be easier to detect in young-TOs because of their smaller distances. We do not believe this effect has a strong impact on the conclusions of this paper, given that there is still a substantial overlap in distances of young-TOs and other LLAGNs. This issue is further discussed in Sections 3.1 and 3.2.

2.3 Spatially resolved spectra: examples and first impressions

Figs 1 and 2 illustrate spatially resolved spectra for a representative subset of the galaxies in our sample. Spatial gradients in spectral properties will be analysed in detail in the remainder of this paper, but some results are evident from a simple visual inspection of these figures.

(i) First, in objects such as the old-LINER NGC 315 the off-nuclear spectra look virtually identical to the nuclear spectrum, implying a high spatial uniformity of the stellar populations. The only noticeable gradient is in the emission lines, which are concentrated in the nucleus.

(ii) Secondly, the strongest gradients are found in systems with conspicuous HOBLs (e.g. NGC 4150 and 4569). As noted above, these are nearly all weak [O I] sources. This combination of youngish stellar population and [O I]/H$\alpha \leqslant 0.25$ fits our definition of young-TOs.

(iii) Thirdly, although HOBLs, when present, are stronger in the central extraction, they are not confined to the nucleus. This is clearly seen in the cases of NGC 4150 and 4569, where HOBLs still show up in extractions more than 3 arcsec away from the nucleus. Given that the seeing in these observations was typically better than 1 arcsec, we conclude that the 'HOBL region' is spatially extended.

(iv) As is typical of LLAGNs, emission lines are generally weak. In fact, many objects show no sign of important diagnostic lines such as Hβ and [O III]λ5007 even in the nucleus. The measurement of emission lines requires careful subtraction of the starlight, which we postpone to a future communication.

3 STELLAR POPULATION GRADIENTS

A convenient way to map spatio-spectral variations is to compute profiles of absorption features and continuum colours along the slit (e.g. Cid Fernandes et al. 1998; Raimann et al. 2003). From Papers I and II we know that an AGN continuum contributes very little (if anything) to our ground-based optical spectra. Any significant

Table 1. Observations and sample properties. The columns show the following: (1) galaxy name; (2) and (3) useful angular and linear coverage; (4) angular scale; (5) and (6) S/N at 4800 Å at nucleus an outer extractions; (7) slit position angle; (8) spectral type according to HFS97; (9) stellar population category (Paper I); (10) equivalent width of the Ca II K band at the nucleus, in Å; (11) W = weak [O I] (i.e. [O I]/H$\alpha \leqslant 0.25$), S = strong [O I] ([O I]/H$\alpha > 0.25$); (12) combined emission-line and stellar population class. Objects marked with a $\star$ were observed at KPNO.

Galaxy (1)	$\theta_{\rm out}$ (arcsec) (2)	$r_{\rm out}$ (pc) (3)	pc/arcsec (4)	$({\rm S/N})_{\rm nuc}$ (5)	$({\rm S/N})_{\rm out}$ (6)	PA (°) (7)	Type (8)	η (9)	$W_{\rm K}^{\rm nuc}$ (10)	[O I] (11)	Class (12)
NGC 0266	4.5	1364	303	40	19	100.4	L1.9	O	18.8	S	Old-LINER
NGC 0315	5.6	1799	319	52	24	94.3	L1.9	O	17.0	S	Old-LINER
NGC 0404*	11.7	136	12	53	24	0.0	L2	I	9.8	W	Young-TO
NGC 0410	4.5	1544	342	61	24	90.5	T2:	O	17.6	W	Old-TO
NGC 0521	4.5	1465	325	51	14	124.3	T2/H:	O	17.9	W	Old-TO
NGC 0718	4.5	468	104	44	26	137.8	L2	I	13.1	W	Young-TO
NGC 0772	6.8	1070	158	57	19	127.1	H/T2:	I	11.6	W	Young-TO
NGC 0841	4.5	1301	288	65	17	51.8	L1.9:	I	14.9	S	Young-LINER
NGC 1052	4.5	389	86	68	41	167.1	L1.9	O	17.3	S	Old-LINER
NGC 1161	6.8	850	126	56	21	37.6	T1.9:	O	19.0	W	Old-TO
NGC 2681	7.3	473	64	41	28	81.5	L1.9	I	12.3	W	Young-TO
NGC 2685	7.9	620	79	40	29	167.3	S2/T2:	I/O	18.7	W	Old-TO
NGC 3166	10.7	1143	107	45	20	188.4	L2	I/O	15.9	S	Old-LINER
NGC 3245	4.5	485	108	66	33	264.5	T2:	I/O	15.2	W	Old-TO
NGC 3627	13.4	427	32	50	32	222.6	T2/S2	I	11.6	W	Young-TO
NGC 3705	5.6	465	82	31	18	218.2	T2	I	14.8	W	Young-TO
NGC 4150	4.5	212	47	42	23	267.6	T2	I	12.6	W	Young-TO
NGC 4438	7.3	597	81	40	25	224.4	L1.9	I/O	17.8	S	Old-LINER
NGC 4569	4.5	367	81	57	27	228.7	T2	I	5.0	W	Young-TO
NGC 4736	17.5	364	21	50	34	324.1	L2	I	12.9	W	Young-TO
NGC 4826	4.5	90	20	42	39	250.5	T2	I	14.4	W	Young-TO
NGC 5005	11.6	1194	103	53	18	286.6	L1.9	I	14.6	S	Young-LINER
NGC 5377	6.8	1017	150	48	18	288.6	L2	I	8.7	W	Young-TO
NGC 5678	7.3	1265	173	53	30	149.5	T2	I	8.7	W	Young-TO
NGC 5921	4.5	551	122	46	13	188.3	T2	I	11.2	W	Young-TO
NGC 5970	7.3	1123	153	32	20	234.1	L2/T2:	I/O	18.4	W	Old-TO
NGC 5982	6.2	1163	188	56	40	311.5	L2::	O	18.1	S	Old-LINER
NGC 5985	4.5	857	190	38	11	308.8	L2	I/O	18.9	S	Old-LINER
NGC 6340*	9.4	998	107	61	18	0.0	L2	O	20.0	S	Old-LINER
NGC 6384	4.5	582	129	40	16	211.3	T2	I/O	18.6	W	Old-TO
NGC 6482	7.3	1859	254	74	28	115.8	T2/S2::	O	18.8	W	Old-TO
NGC 6500	4.5	868	192	50	14	197.2	L2	I/O	15.8	W	Old-TO
NGC 6501	4.5	866	192	59	20	240.2	L2::	O	16.8	S	Old-LINER
NGC 6503	13.4	395	30	40	26	10.1	T2/S2:	I	9.5	W	Young-TO
NGC 6702	4.5	1373	304	55	17	335.5	L2::	O	18.1	S	Old-LINER
NGC 6703*	9.4	1629	174	55	33	0.0	L2::	O	18.5	S	Old-LINER
NGC 6951	4.5	527	117	39	30	0.0	S2/L	I/O	16.4	W	Old-TO
NGC 7177*	11.7	1032	88	55	27	0.0	T2	I/O	16.6	W	Old-TO
NGC 7217*	11.7	908	78	48	25	0.0	L2	O	19.2	W	Old-TO
NGC 7331*	16.4	1136	69	57	39	0.0	T2	O	18.0	W	Old-TO
NGC 7626	4.5	997	221	71	35	122.6	L2::	O	18.1	W	Old-TO
NGC 7742*	11.7	1259	108	47	32	0.0	T2/L2	I/O	17.1	W	Old-TO
NGC 3367	4.5	953	211	88	15	203.6	H	Y	2.6	–	–
NGC 0224	7.9	27	3	60	66	66.5	Normal	O	17.5	–	–
NGC 0628	6.2	292	47	40	25	167.3	Normal	I/O	16.1	–	–
NGC 1023	7.9	402	51	59	35	293.7	Normal	O	19.4	–	–
NGC 2950	5.6	637	113	44	24	48.5	Normal	O	17.4	–	–

variation detected in these properties can thus be confidently attributed to variations in the stellar populations.

In Paper I we have measured an extensive set of stellar population indices in different systems. In this paper we will use the equivalent widths of the Ca II K line ($W_{\rm K}$), the G band ($W_{\rm G}$), Mg I ($W_{\rm Mg}$) and $W_{\rm C}$ (a 'pseudo-equivalent width' centred in the continuum just to the blue of H9) plus the $C_{3660} \equiv 3660/4020$ and $C_{5313} \equiv 5313/4020$ continuum colours, all measured in the Bica system. The 4000-Å break index of Balogh et al. (1999), $D_n(4000)$, is also used, but only for illustrative purposes. The $W_{\rm C}$ index works as a direct tracer of HOBLs: spectra with clearly visible HOBLs all have $W_{\rm C} < 3.5$ Å, while spectra dominated by old populations ($\sim 10^{10}$ yr) have larger $W_{\rm C}$ due to a blend of metal lines. As shown in Paper I, $W_{\rm K}$, which is a much stronger and thus more robust feature, is also a good (albeit

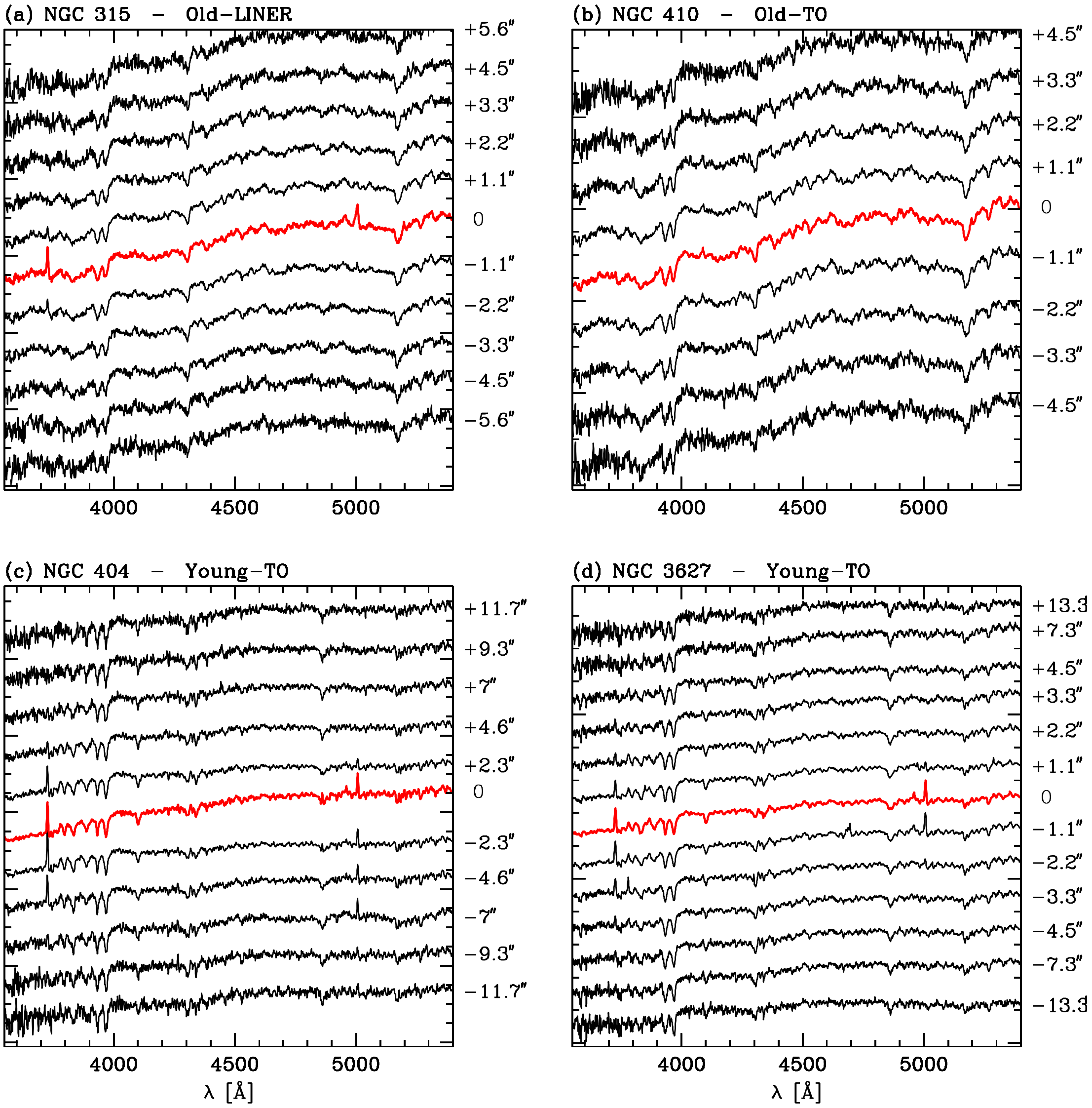

Figure 1. Examples of spatially resolved spectra of LLAGNs. Spectra have been normalized and shifted for clarity. The nuclear spectrum is drawn with a thicker line. Labels on the right indicate the angular distance from the nucleus.

indirect) tracer of the intermediate age populations responsible for the HOBLs.

All these indices are highly correlated (Paper I). Their radial behaviours however need not be the same. For instance, a compact blue source such as a young or intermediate age starburst should produce a larger dilution at the nucleus of the bluer indices, such as $W_{\rm K}$, than of the redder ones, such as $W_{\rm Mg}$. The comparison of the $W_{\rm K}$ and $W_{\rm Mg}$ profiles may thus allow inferences about the nuclear stellar population.

We have measured these indices automatically for all 521 extractions analysed in this work following the recipes outlined in Paper I for Bica indices and in Balogh et al. (1999) for $D_n(4000)$. This served as a further test of the objective pseudo-continuum definition proposed in Paper I. After visual inspection of the results, we have judged that only in 18 spectra (3 per cent of the total) did the pseudo-continuum deserve corrections. Uncertainties in all spectral indices were estimated by means of Monte Carlo simulations. The typical uncertainties at $\theta = \pm 4.5$ arcsec, the outermost extractions in many of our sources, are 0.5–1 Å for all equivalent widths, and 0.04 for C_{3660}, C_{5313} and $D_n(4000)$. Indices for the nuclear extractions are two to three times more accurate.

3.1 Radial profiles of stellar indices

Figs 3–12 show the variations of our seven stellar population indices with angular distance from the nucleus for some illustrative cases. The top panels show $W_{\rm K}$ (black, solid line), $W_{\rm C}$ (magenta, thin line), $W_{\rm G}$ (green, dotted line) and $W_{\rm Mg}$ (red, dashed line). The middle panels show the C_{3660} (blue, dotted line) and C_{5313} (black, solid line) colours, plus the $D_n(4000)$ profile (green, dashed line). The slit brightness profile $S(r)$ at $\lambda = 4200$ Å is plotted in the bottom panel to give an idea of the light concentration. The thick line segment marks the FWHM of $S(r)$; its value is listed in the top right in both angular and linear units. A stellar profile is also plotted to illustrate the spatial resolution. Vertical dotted and dashed lines indicate projected distances of ±100 and ±500 pc from the nucleus, respectively.

The examples in Figs 3–12 were chosen to illustrate the variety of radial profiles found in the sample. In a first cut, the W_λ profiles may be grouped into three categories:

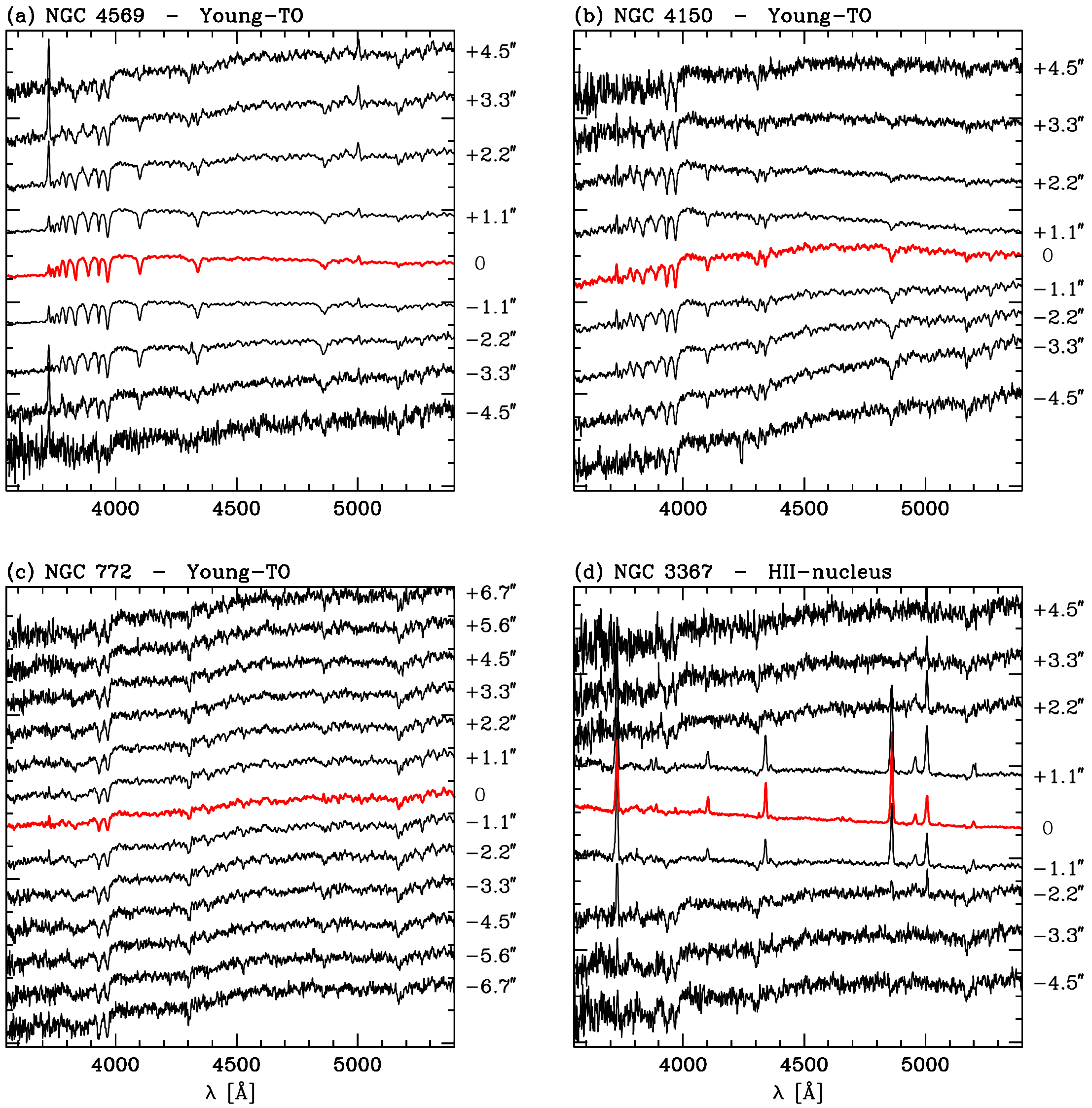

Figure 2. As Fig. 1.

(i) flat (e.g. NGC 305 and 410);
(ii) centrally peaked (e.g. NGC 7742);
(iii) 'diluted' profiles (e.g. NGC 3627 and 4569).

Most objects studied here have either flat or diluted W_λ profiles. In NGC 6951 and 7742, the peaked appearance of $W_\lambda(r)$ is due to circumnuclear star-forming rings which appear in our outermost extractions (Pérez et al. 2000). Outside these rings, the absorption lines rise up again, as in NGC 1097 and other ringed galaxies studied by Cid Fernandes et al. (1998).

The main focus of our analysis throughout the rest of this paper will be on the nature and properties of the source of dilution in LLAGNs with diluted profiles. These profiles cannot be explained in terms of metallicity gradients, as this should produce peaked profiles. The drop in W_λ towards the nucleus in these galaxies is thus clearly the result of dilution of the metallic features by a centrally concentrated stellar population which is younger than that a few arcsec away from the nucleus. The most dramatic example of this effect is seen in the starburst galaxy NGC 3367, where the young starburst appears only in the three central extractions (Fig. 12). We note in passing that, at $d = 43.6$ Mpc, this galaxy is one of the most distant in our sample, well above the median distance of 27.9 Mpc. Yet, its W_λ gradients are clearly mapped with our data, which shows that the worries raised in Section 2.2 about possible distance related biases are not justified in practice. Similar comments apply to NGC 5678 (Fig. 7; $d = 35.6$ Mpc) and NGC 772 (Fig. 11; $d = 32.6$ Mpc).

In LLAGNs with diluted profiles, the diluting agent could in principle also be a young starburst, but, as shown in Papers I and II, in only ~10 per cent of LLAGNs does such a young component contribute more than 10 per cent of the flux at 4020 Å in our ground-based nuclear spectra. For most objects, the radial dilution is caused mainly by an intermediate age population, which appears far more frequently and in much larger strengths. These populations are easily recognized by their weak metal lines and deep HOBLs, as seen, for instance, in NGC 3627 and 4569 (Figs 1, 2, 8 and 10).

Figs 13–15 show the W_K profiles for all 47 galaxies in our sample, sorted in an increasing sequence of nuclear W_K values. This ordering bears an excellent correspondence with the profile shapes: of the first 19 galaxies (from NGC 3367 to 6500), at least 16 have diluted W_K profiles. The exceptions are NGC 2681, 841 and possibly 6500.

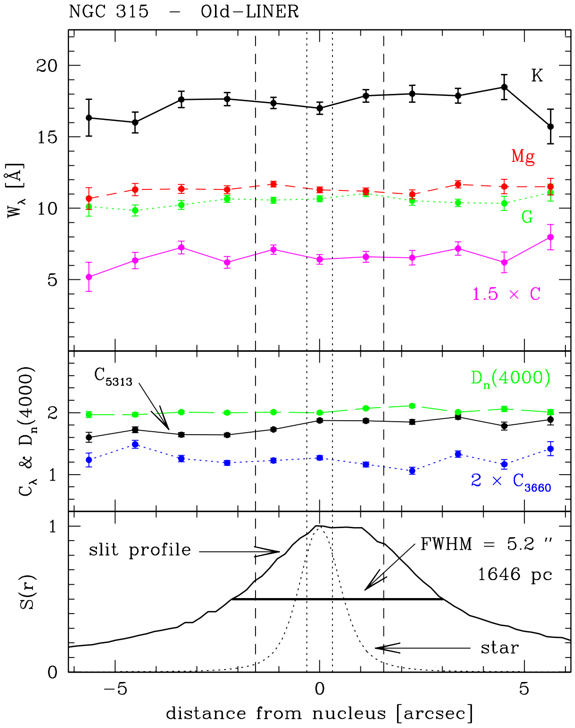

Figure 3. Spatial variations of stellar population indices for NGC 315. Top: radial profiles of $W_{\rm K}$ (black, thick solid line), $W_{\rm C}$ (magenta, thin line), $W_{\rm G}$ (green, dotted line) and $W_{\rm Mg}$ (red, dashed line). Note that $W_{\rm C}$ has been multiplied by 1.5 for clarity. Middle: radial profile of the 3660/4020 (blue, dotted line) and 5313/4020 (black, solid line) colours, and $D_n(4000)$ (green, dashed line). The 3660/4020 colour is multiplied by 2 in the plot. Bottom: surface brightness at 4200 Å (in flux units) along the slit, normalized to $S(r = 0) = 1$. The FWHM of the slit profile is marked as a thick line segment, and listed at the top right in both arcsec and pc. The dotted line shows the instrumental profile, corresponding to a star observed on the same night. Dotted and dashed vertical lines indicate projected distances of ± 100 and 500 pc from the nucleus, respectively.

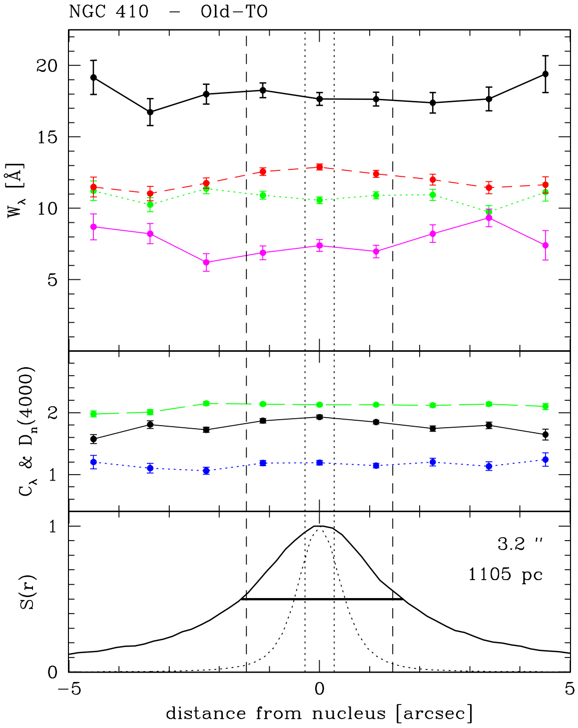

Figure 4. As Fig. 3, but for NGC 410.

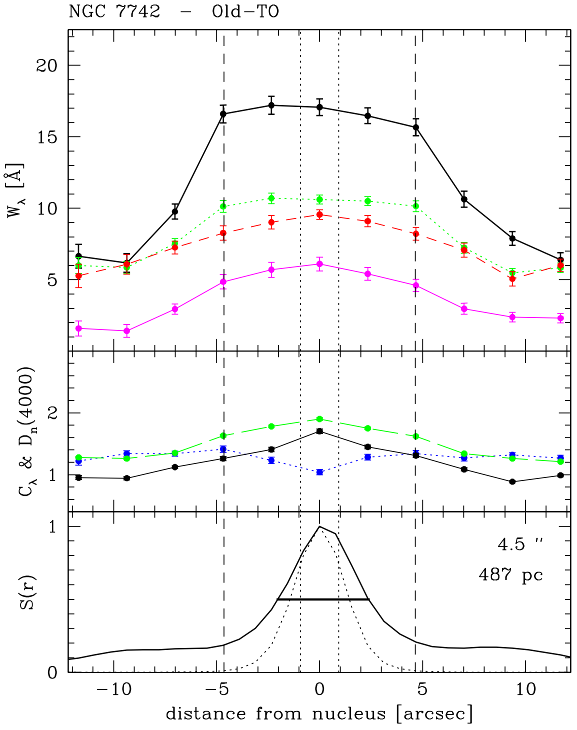

Figure 5. As Fig. 3, but for NGC 7742.

From NGC 3166 onwards, i.e. for $W_{\rm K}^{\rm nuc} > 15$–16 Å, profiles are either centrally peaked or, more commonly, approximately flat. This obvious link is examined in quantitative terms in the next section.

3.2 Gradients in equivalent widths

In order to quantify the spatial gradients seen in Figs 3–15 we define a radial dilution index

$$\delta_\lambda = \frac{W_\lambda^{\rm off} - W_\lambda^{\rm nuc}}{W_\lambda^{\rm off}}, \tag{1}$$

which compares nuclear and mean off-nuclear equivalent widths. Flat W_λ profiles should yield $\delta_\lambda \sim 0$, while $\delta_\lambda < 0$ correspond to centrally peaked profiles and $\delta_\lambda > 0$ to diluted profiles. Furthermore, if the nuclear spectrum differs from that in off-nuclear extractions only by an extra continuum source (or, more precisely, a source with negligible W_λ), then δ_λ measures the fractional contribution of this source to the continuum at λ (Cid Fernandes et al. 1998).

$W_\lambda^{\rm off}$ is defined as the average of $W_\lambda(\theta)$ for extractions centred at $|\theta|$ between 2.2 and 4.7 arcsec from the nucleus. Note that for the NOT observations this definition excludes extractions adjacent to the nucleus, which in some cases are contaminated by nuclear light due to seeing. The averaging is carried out weighting by the error in W_λ. The uncertainties in the dilution index were evaluated from standard error propagation. Typical 1σ uncertainties in δ_λ are 0.1 for $W_{\rm C}$ and 0.04 for $W_{\rm K}$, $W_{\rm G}$ and $W_{\rm Mg}$. We have also explored an alternative definition of $W_\lambda^{\rm off}$ in terms of extractions between $r = 250$ and 750 pc from the nucleus. However, this turned out to yield similar results, which further demonstrates that our conclusions are not significantly affected by potential distance-related biases (Section 2.2).

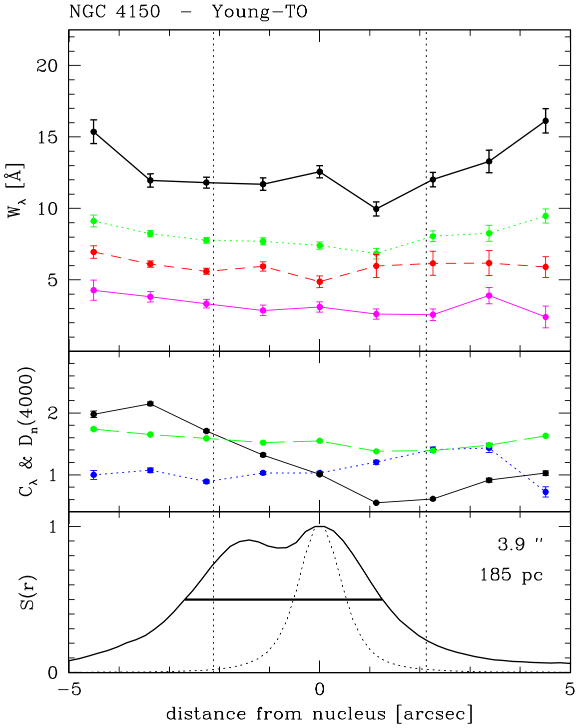

Figure 6. As Fig. 3, but for NGC 4150.

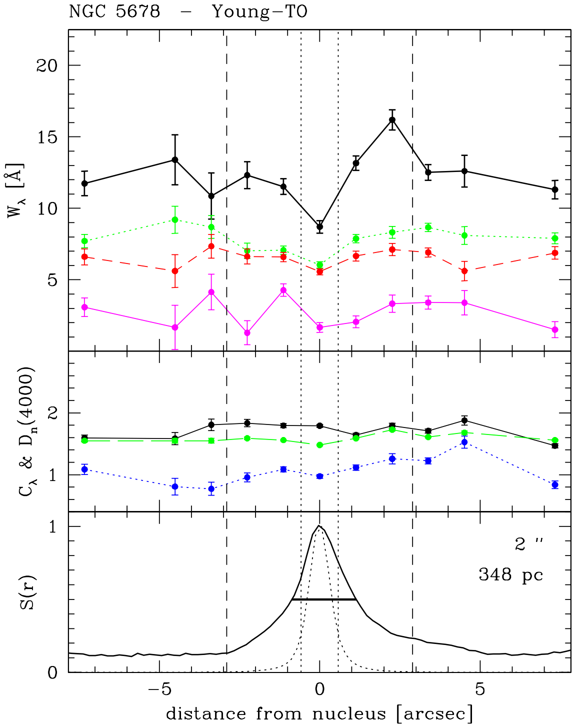

Figure 7. As Fig. 3, but for NGC 5678.

Table 2 lists the resulting values of δ_λ. Gradients are considered to be significant whenever $|\delta_K| > 10$ per cent, which corresponds to a $\sim 2.5\sigma$ detection limit. According to this criterion, significantly diluted profiles ($\delta_K > 10$ per cent) occur in 13 of the 42 LLAGNs in our sample, while only three have significantly peaked profiles ($\delta_K < -10$ per cent). Spatially homogeneous stellar populations therefore prevail among LLAGNs, accounting for ∼60 per cent of our sample.

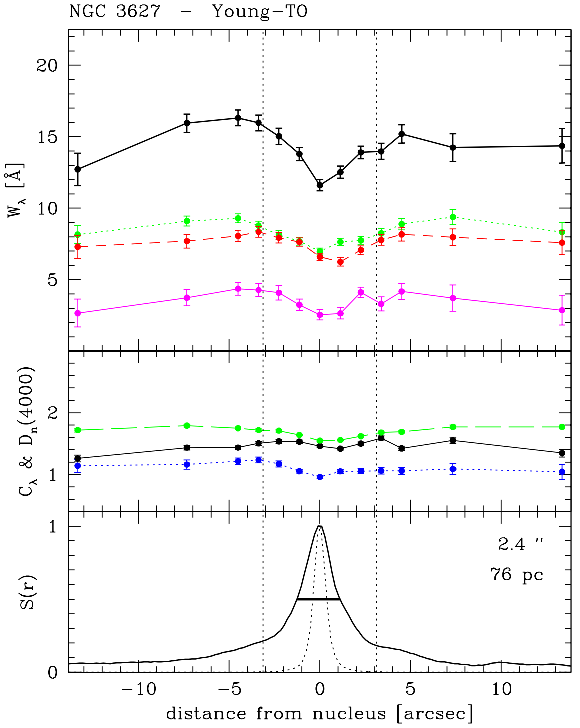

Figure 8. As Fig. 3, but for NGC 3627.

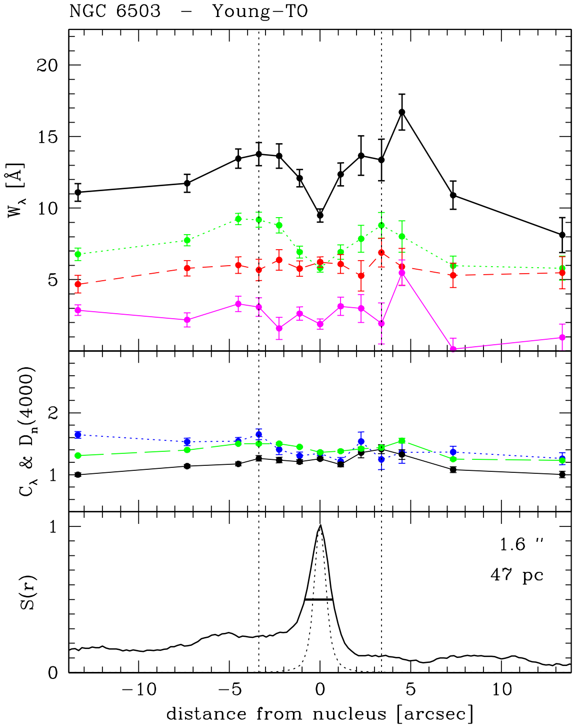

Figure 9. As Fig. 3, but for NGC 6503.

3.2.1 Relations between W_λ gradients, emission-line and nuclear stellar population properties

In Fig. 16 we investigate the relation between dilution and nuclear stellar population by plotting δ_λ against $W_\lambda^{\rm nuc}$ for $W_{\rm C}$, $W_{\rm K}$, $W_{\rm G}$ and

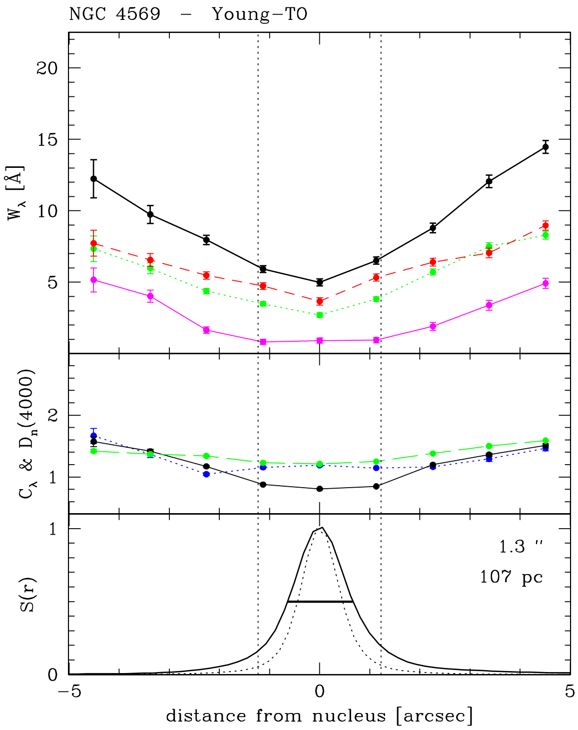

Figure 10. As Fig. 3, but for NGC 4569.

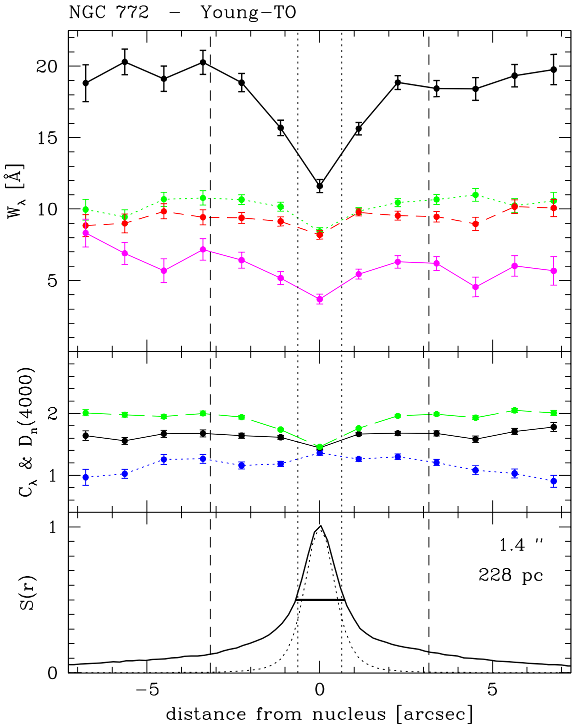

Figure 11. As Fig. 3, but for NGC 772.

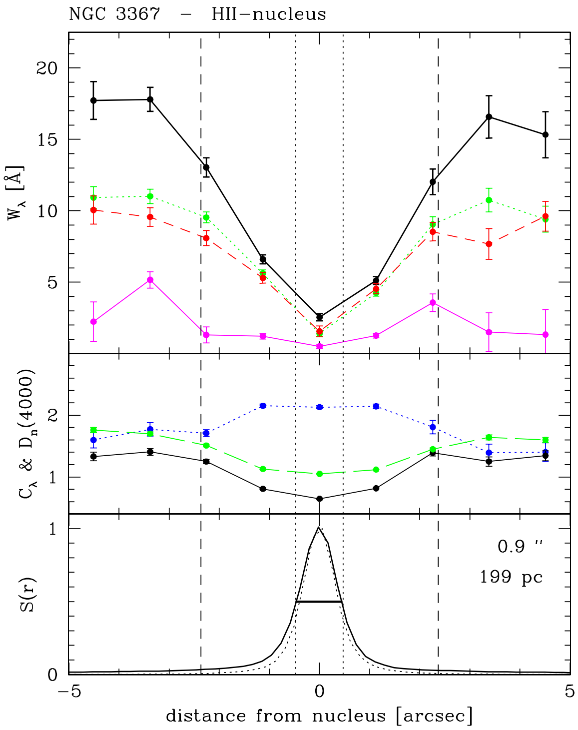

Figure 12. As Fig. 3, but for NGC 3367, a starburst galaxy in our comparison sample.

W_{Mg}. The vertical dotted lines in this plot are the same as those used in Paper I to approximately distinguish objects with significant intermediate age populations (those with $W_{\mathrm{C}} \lesssim 3.5$, $W_{\mathrm{K}} \lesssim 15$, $W_{\mathrm{G}} \lesssim 9$ and $W_{\mathrm{Mg}} \lesssim 9$ Å, which are classed as $\eta = \mathrm{I}$) from those dominated by older populations ($\eta = \mathrm{I/O}$ and O). Fig. 16 shows that these dividing lines also segregate objects with significant dilution from those without. Focusing on the $W_{\mathrm{K}}^{\mathrm{nuc}} = 15$ Å limit, which separates young from old sources in our simple classification scheme, we find that 12 out of the 13 objects with $\delta_{\mathrm{K}} > 10$ per cent fall into the young category, the exception being NGC 3245, which, with $W_{\mathrm{K}}^{\mathrm{nuc}} = 15.2 \pm 0.3$ Å, sits right at the border line between young and old sources. In other words, galaxies with significant radial gradients in their stellar populations contain intermediate age populations in their nuclei. The converse is also true, as at least 12 out of 16 young-LLAGNs have diluted profiles. This is the same result found in Figs 13–15, where we see that virtually every galaxy with $W_{\mathrm{K}}^{\mathrm{nuc}} \lesssim 15$ Å has a diluted W_{K} profile.

Because in Papers I and II we have shown that nearly all nuclei with weak metal absorption lines are weak [O I] emitters, we expect that the strong relation between δ_λ and W_λ^{nuc} seen in Fig. 16 translates to an equally strong relation between δ_λ and [O I]/Hα. This is confirmed in Fig. 17, which shows that all but one object with $\delta_{\mathrm{K}} > 10$ per cent have [O I]/H$\alpha < 0.25$. Two other weak [O I] nuclei, NGC 404 and 4150, should probably be included in the list of sources with diluted profiles. NGC 404 is so close by (2.4 Mpc) that our outer useful extractions do not reach a probable rise in W_λ for larger radii, if this indeed happens in this dwarf galaxy. Dust effects may also be present, as indicated by the peak in the C_{5313} colour in the nucleus of NGC 404 (Fig. 19). In NGC 4150 the strongest dilution is seen at $\theta = +1.1$ arcsec from the nucleus, and the rise in W_λ seen in our last extractions has a small weight in our definition of W_λ^{off}, resulting in a small δ_λ. This asymmetry is associated with the pronounced nuclear dust lane in this galaxy (Paper II), which is responsible for its asymmetric C_{5313} profile (Fig. 6).

The only strong [O I] source with significant radial dilution is NGC 5005 ($\delta_{\mathrm{K}} = 11 \pm 3$ per cent, [O I]/H$\alpha = 0.65$). Given that this nucleus is classified as an L1.9 by HFS97, it is conceivable that the dilution is caused by a nuclear featureless continuum, as found in spatially resolved spectroscopy of type 1 Seyferts (Cid Fernandes et al. 1998). However, none of the other seven type 1 LLAGNs in our sample exhibits significant dilution. Furthermore, HOBLs

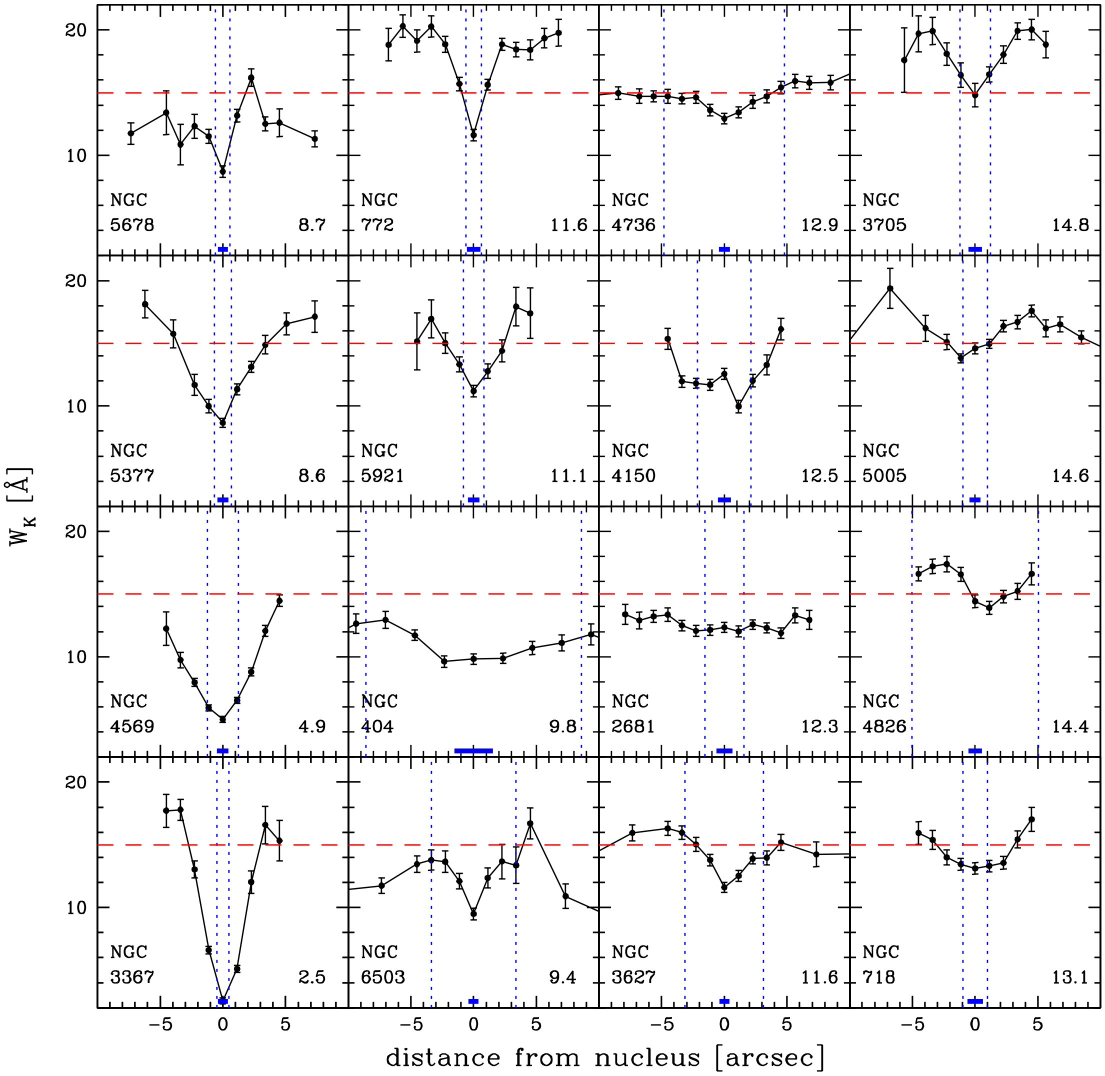

Figure 13. Radial profiles of the equivalent width of the Ca II K line for all galaxies in the sample. Dotted vertical lines mark distances of ±100 pc from the nucleus. A horizontal dashed line is drawn at $W_{\rm K} = 15$ Å for reference. The thick line segment in the bottom of each panel indicates the seeing, measured from the FWHM of star observed on the same night. Objects are sorted by the value of $W_{\rm K}$ at the nucleus ($W_{\rm K}^{\rm nuc}$), indicated in the bottom-right corner of each panel. Galaxies in this figure have $W_{\rm K}^{\rm nuc}$ between 2.5 (bottom left-hand panel) and 14.8 Å (top right).

are clearly present in the nuclear spectrum of NGC 5005, so we favour the interpretation that, as in other objects, dilution is caused mainly by a centrally concentrated intermediate age population. As noted in Paper II, and confirmed by our radial dilution analysis, the contribution of a non-stellar continuum to our ground-based spectra is negligible. Clear signatures of a featureless continuum in LLAGNs are only found under the much higher spatial resolution of the *HST*, and even then they are rare.

We thus conclude that virtually all sources with radially diluted metal lines are weak [O I] emitters. Note, however, that the converse is not true, as there are several weak [O I] objects with either flat or, more rarely, peaked W_λ profiles. These non-diluted weak [O I] nuclei are dominated by old stellar populations, as deduced from their strong metal lines (Fig. 16; Paper I).

To summarize, combining the relations between dilution, stellar population and emission-line properties we find that significant stellar populations gradients are found almost exclusively in young-TOs, i.e. objects with weak [O I] and a conspicuous intermediate age nuclear stellar population. Old-TOs and old-LINERs, on the other hand, tend to have spatially uniform stellar populations. These strong relations can be visualized comparing the location of different symbols in Figs 16 and 17.

3.2.2 W_λ gradients and the colour of the nuclear source

Another result of the $W_\lambda(r)$ analysis is that the spatial dilution, when significant, tends to be larger for shorter wavelengths, which implies that the diluting agent is bluer than the off-nuclear stellar population. This is illustrated in Fig. 18, where we plot the dilution in the K line (central $\lambda = 3930$ Å) against the dilution in $W_{\rm C}$ ($\lambda = 3816$ Å), $W_{\rm G}$ ($\lambda = 4301$ Å) and $W_{\rm Mg}$ ($\lambda = 5176$ Å). For LLAGNs with $\delta_{\rm K} \gtrsim 10$ per cent, the dilution follows a wavelength sequence: $\delta_{\rm C} > \delta_{\rm K} > \delta_{\rm G} > \delta_{\rm Mg}$. (Deviations from this sequence are all within the uncertainties in δ_λ.) Some objects with clear gradients in K show little, if any, dilution in Mg I (e.g. NGC 3245 and 6503). In NGC 772 and 4569 and other objects, the colour profiles confirm the existence of the blue nuclear component inferred from the behaviour of δ_λ for different lines. In others, however, $C_\lambda(r)$ shows little

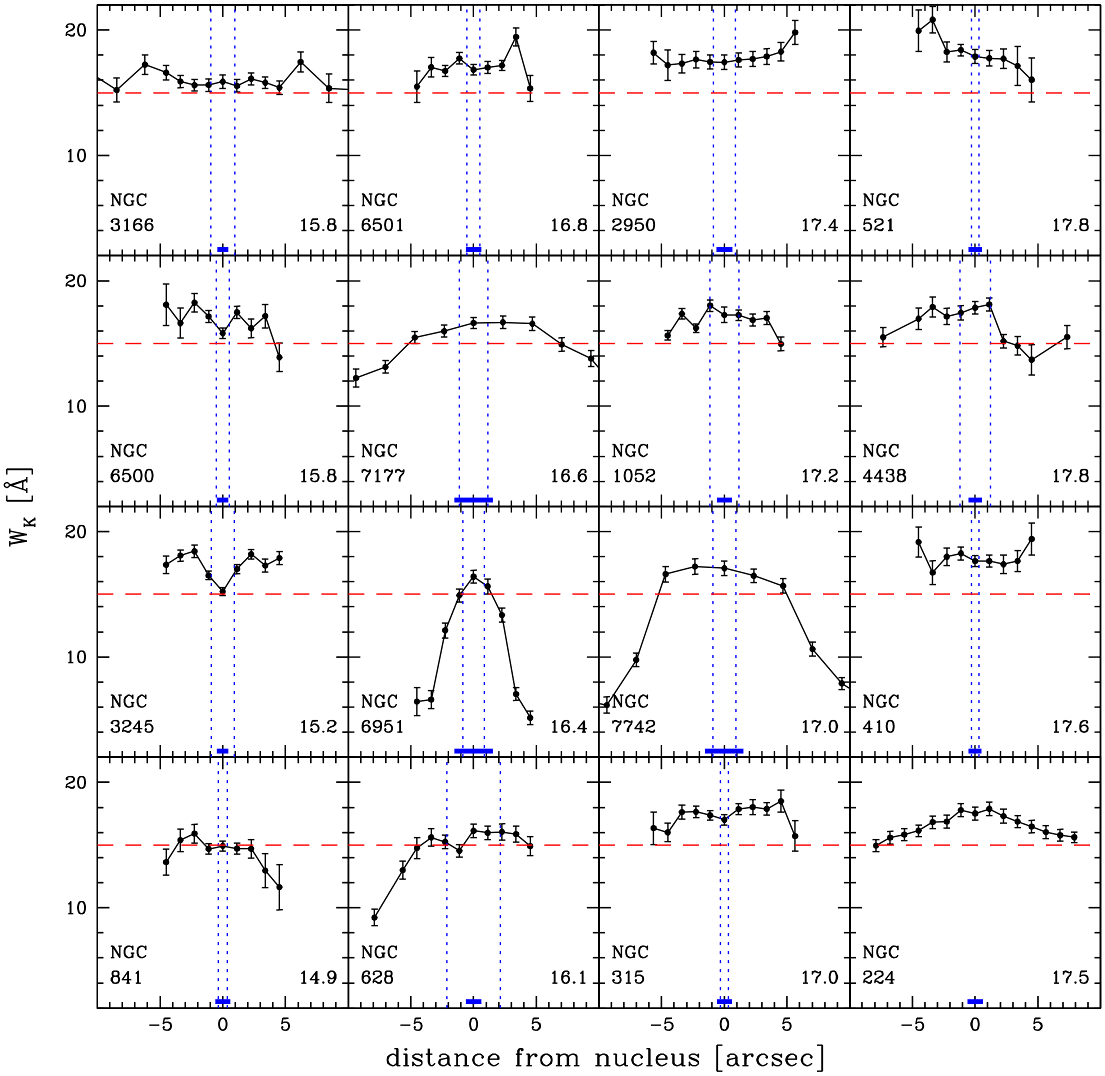

Figure 14. As Fig. 13, but for galaxies with $W_{\rm K}^{\rm nuc}$ between 14.9 and 17.8 Å.

variation (e.g. NGC 3627) or even slightly redder colours in the nucleus (NGC 3245), contrary to the inference from the absorption-line gradients. As discussed below, this apparent contradiction is due to dust in the central regions of these galaxies.

3.3 Colour gradients and extinction

Colour gradients carry information on the variations of stellar populations and extinction across a galaxy. Our C_{3660} colour brackets the region containing the 4000-Å break and Balmer jump, while C_{5313} is roughly equivalent to B–V. Because of the larger wavelength interval involved (5313–4020 Å) and the absence of spectral discontinuities in this range, C_{5313} is the more reddening sensitive of the two indices. One must nevertheless bear in mind that a $C_{5313}(r)$ profile cannot be trivially transformed into an extinction profile without a simultaneous analysis of stellar population variations.

Figs 19–21 show the C_{3660} (dotted, blue line) and C_{5313} (solid, black line) colour profiles, also ordered according to $W_{\rm K}^{\rm nuc}$. Centrally peaked $C_{5313}(r)$ profiles are apparently rare among galaxies with $W_{\rm K}^{\rm nuc} \lesssim 15$ Å (Fig. 19), with exceptions (e.g. NGC 404, 718 and 3245). This type of profile appears more often in Figs 20 and 21, which contain galaxies with $W_{\rm K}^{\rm nuc} \gtrsim 15$ Å.

In order to examine colour gradients in more quantitative terms we compute the ratio $C_{5313}^{\rm nuc}/C_{5313}^{\rm off}$ between the values of C_{5313} in the nucleus and a mean off-nuclear colour, defined as the weighted average of extractions between $|\theta| = 2.2$ and 4.7 arcsec (as done for $W_{\lambda}^{\rm off}$ in Section 3.2). This ratio can be transformed into the index

$$\delta_V = 5.98 \log \left(\frac{C_{5313}^{\rm nuc}}{C_{5313}^{\rm off}} \right) \qquad (2)$$

which measures by how many V-band magnitudes one has to deredden the nuclear spectrum to make it match the off-nuclear C_{5313} colour. The coefficient in this equation comes from assuming the Cardelli et al. (1989) extinction curve with $R_V = 3.1$, which we do throughout this paper. $\delta_V < 0$, which indicates a bluening towards the nucleus, is henceforth referred to as a 'blue gradient', while $\delta_V > 0$ is called a 'red gradient'. Colour gradients were also examined by fitting the nuclear spectrum with a combination of off-nuclear spectra plus reddening, which yields the nuclear extinction relative to that of the off-nuclear extractions. This method gives essentially identical results to those based solely on the C_{5313} colour, with a mean offset of just 0.04 mag and rms difference of 0.16 mag between the two δ_V estimates.

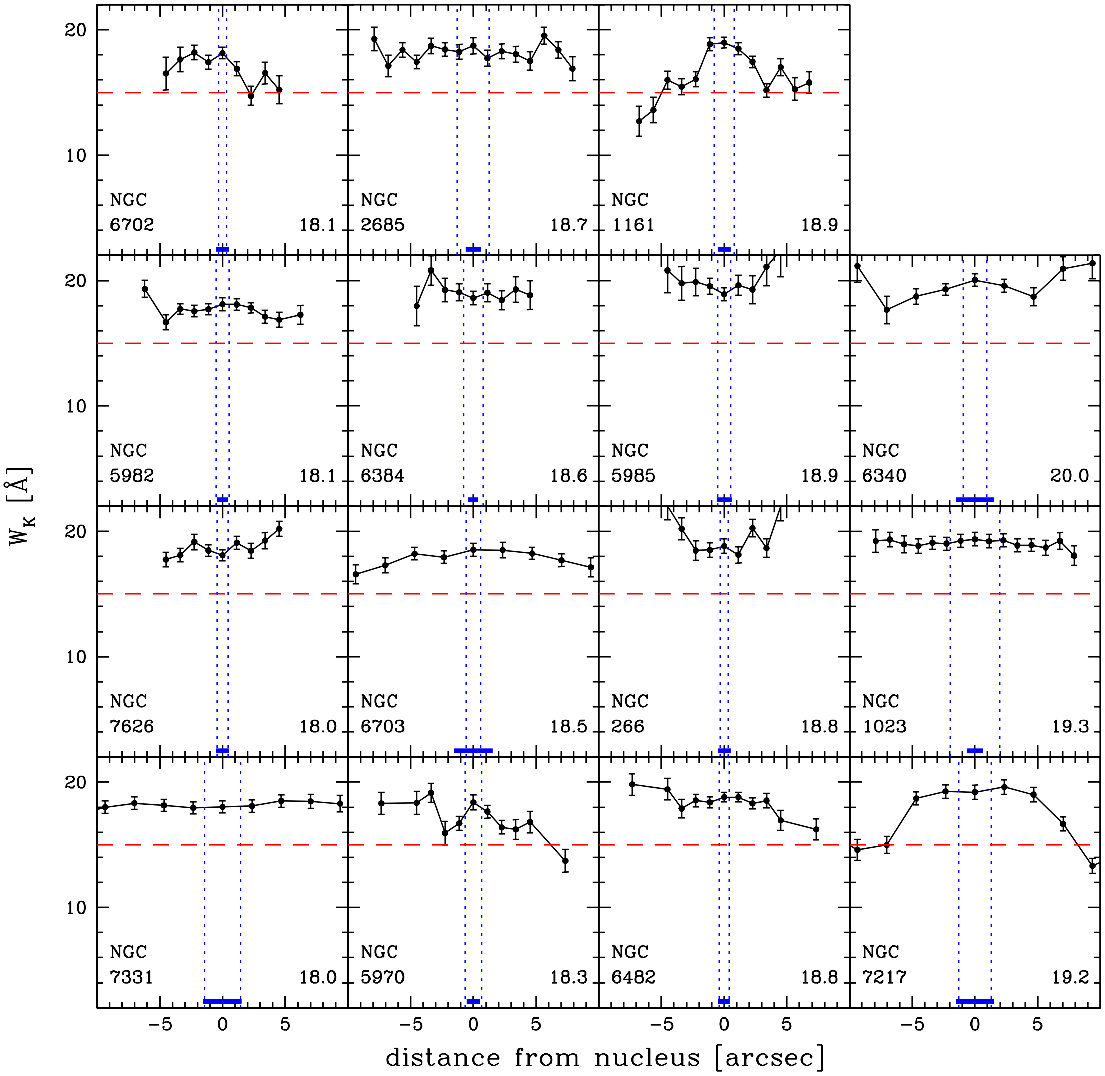

Figure 15. As Fig. 13, but for galaxies with W_K^{nuc} between 18 and 20 Å.

Fig. 22 compares δ_V with δ_K, W_K^{nuc} and [O I]/Hα. The figure confirms that red gradients are more common for objects with $W_K^{nuc} > 15$ Å, i.e. among old-LLAGNs, which also tend to have flat W_λ profiles. In fact, the plot shows that all objects with $W_K^{nuc} > 15$ Å, all strong [O I] sources and all but one of the $\delta_K < 10$ per cent objects have red gradients, the exception being NGC 4150, a young-TO for which, as discussed above, δ_K is underestimated. On the other hand, galaxies with significantly diluted W_λ profiles, ∼90 per cent of which are young-TOs, have both blue and red gradients. Of the 13 LLAGNs with $\delta_K > 10$ per cent, eight have blue gradients and five have red gradients, but note that in several of these objects the colour gradient is negligible, with $|\delta_V| < 0.1$ mag.

Because colours per se do not disentangle intrinsic stellar population properties from extinction, these estimates of δ_V can only be interpreted as actual spatial variations in dust content in the absence of stellar population variations. This is a reasonable assumption for objects with relatively flat W_λ profiles (and thus spatially uniform stellar populations), which, as shown above, are essentially all old-LINERs and old-TOs. The red gradients observed in these objects can thus be safely attributed to extinction gradients. Note, however, that most objects with $\delta_K \sim 0$ cluster around values of δ_V of 0.1–0.4 mag, indicating that extinction gradients tend to be small.

The assumption of spatially uniform stellar populations breaks down for galaxies with diluted or peaked W_λ profiles. In the latter case, one expects δ_V to overestimate the extinction gradient, as the reference off-nuclear extractions sample a younger population than that present in the nucleus. This is clearly the case of NGC 6951, for which we obtain $\delta_V = 1.2$ mag, the largest value in the whole sample. This effect is responsible for at least part of the trend of increasing of δ_V as δ_K becomes more negative (Fig. 22a). Conversely, when the nucleus contains a younger (and thus intrinsically bluer) population than off-nuclear positions, the resulting δ_V should be regarded as a *lower limit* to the actual variation in A_V. From Section 3.2 and Fig. 18 we know that in galaxies with diluted W_λ profiles the diluting source is intrinsically bluer than off-nuclear spectra, which should lead to blue gradients. While some of these galaxies indeed have blue gradients, most (9/13) have negligible or slightly red gradients, *which can only be understood in terms of a higher dust content in the nucleus.* Hence, contrary to the first impression derived from the relative rarity of centrally peaked C_{5313} profiles among these sources, extinction gradients seem to be a common feature of young-TOs.

In summary, this empirical analysis shows that extinction gradients are present in LLAGNs of all kinds. In old-LINERs and

Table 2. Radial dilution, colour gradients and sizes. The columns show the following: (2)–(5) dilution of the equivalent widths $W_{\rm C}$, $W_{\rm K}$, $W_{\rm G}$ and $W_{\rm Mg}$; (6) gradient in the C_{5313} colour (see equation 2); (7) and (8) HWHM of the flux profile along the slit, in angular and linear units.

NGC (1)	$\delta_{\rm C}$ (per cent) (2)	$\delta_{\rm K}$ (per cent) (3)	$\delta_{\rm G}$ (per cent) (4)	$\delta_{\rm Mg}$ (per cent) (5)	δ_V (mag) (6)	R_S (arcsec) (7)	R_S (pc) (8)
0266	2 ± 9	6 ± 3	3 ± 3	−6 ± 3	0.18 ± 0.07	1.4	435
0315	4 ± 6	3 ± 3	−3 ± 2	1 ± 2	0.17 ± 0.04	2.6	822
0404	7±15	6 ± 4	15 ± 3	9 ± 6	0.54 ± 0.04	2.1	25
0410	8 ± 6	1 ± 3	2 ± 3	−11 ± 3	0.29 ± 0.05	1.6	552
0521	0 ± 9	3 ± 4	2 ± 3	1 ± 3	0.09 ± 0.07	1.1	371
0628	−11 ± 13	−4 ± 4	2 ± 4	0 ± 7	0.22 ± 0.07	7.2	339
0718	21 ± 9	12 ± 3	5 ± 3	0 ± 5	0.24 ± 0.05	1.4	143
0772	39 ± 6	39 ± 3	21 ± 3	13 ± 4	-0.36 ± 0.05	0.7	111
0841	10 ± 10	−3 ± 4	0 ± 4	−7 ± 5	0.37 ± 0.06	1.1	310
1023	−11 ± 7	−2 ± 3	−3 ± 3	−8 ± 2	0.29 ± 0.05	1.9	97
1052	−30±12	−6 ± 4	1 ± 3	−8 ± 3	0.79 ± 0.06	1.3	112
1161	−62±11	−17 ± 3	−17 ± 3	−10 ± 2	0.56 ± 0.05	1.2	151
2681	17±11	1 ± 4	3 ± 4	−4 ± 6	0.11 ± 0.04	1.6	101
2685	−18 ± 9	−4 ± 4	−7 ± 3	−20 ± 6	0.43 ± 0.07	2.4	188
2950	−8 ± 9	2 ± 4	−3 ± 3	−14 ± 4	0.26 ± 0.06	1.6	184
3166	6 ± 9	0 ± 4	−6 ± 4	−11 ± 5	0.03 ± 0.05	1.7	179
3245	10 ± 5	15 ± 2	11 ± 2	−6 ± 2	0.28 ± 0.04	1.0	110
3367	82 ± 6	83 ± 2	86 ± 2	82 ± 4	−1.86 ± 0.06	0.4	95
3627	38 ± 9	23 ± 3	18 ± 3	16 ± 4	−0.06 ± 0.04	1.2	38
3705	28 ± 13	23 ± 5	18 ± 5	17 ± 6	0.25 ± 0.09	0.7	59
4150	8 ± 12	3 ± 4	11 ± 3	20 ± 7	−0.73 ± 0.05	2.0	93
4438	−17 ± 10	−11 ± 4	−7 ± 3	−9 ± 3	1.14 ± 0.05	2.8	227
4569	70 ± 6	52 ± 2	57 ± 3	47 ± 4	−1.24 ± 0.03	0.6	53
4736	11 ± 9	12 ± 3	10 ± 3	5 ± 4	−0.10 ± 0.05	1.1	24
4826	23 ± 9	11 ± 3	8 ± 3	2 ± 4	−0.06 ± 0.05	1.0	20
5005	24 ± 8	11 ± 3	15 ± 3	19 ± 3	0.17 ± 0.05	1.1	109
5377	38 ± 7	37 ± 3	20 ± 3	−3 ± 5	−0.41 ± 0.05	0.8	116
5678	44 ± 13	34 ± 4	27 ± 3	17 ± 4	0.03 ± 0.05	1.0	170
5921	34 ± 9	29 ± 4	22 ± 4	16 ± 6	−0.38 ± 0.07	1.0	116
5970	4 ± 8	−7 ± 4	−2 ± 4	−15 ± 7	0.30 ± 0.07	3.2	496
5982	−5 ± 7	−4 ± 3	−3 ± 3	−8 ± 3	0.13 ± 0.05	1.2	227
5985	−4 ± 12	7 ± 4	0 ± 4	−2 ± 6	0.49 ± 0.08	1.5	294
6340	−9 ± 8	−5 ± 3	−8 ± 3	−9 ± 3	0.96 ± 0.05	3.1	326
6384	−21 ± 10	3 ± 4	8 ± 3	−9 ± 5	0.49 ± 0.07	2.4	316
6482	−8 ± 6	−3 ± 3	−6 ± 2	−13 ± 2	0.43 ± 0.04	1.2	298
6500	13 ± 7	6 ± 3	10 ± 3	−4 ± 3	0.07 ± 0.06	1.0	199
6501	−47 ± 13	1 ± 3	6 ± 2	−4 ± 2	0.34 ± 0.05	1.1	220
6503	39 ± 13	32 ± 4	34 ± 4	−3 ± 8	−0.02 ± 0.06	0.8	23
6702	−22 ± 10	−9 ± 4	−16 ± 4	−18 ± 4	0.07 ± 0.06	1.1	332
6703	−8 ± 8	−2 ± 3	−1 ± 3	−8 ± 3	0.35 ± 0.06	2.1	369
6951	−222 ± 46	−90 ± 8	−54 ± 5	−50 ± 4	1.21 ± 0.05	3.7	435
7177	−11 ± 9	−3 ± 3	−2 ± 3	−5 ± 4	0.28 ± 0.05	4.6	404
7217	−8 ± 8	0 ± 3	1 ± 3	−9 ± 3	0.53 ± 0.06	2.9	221
7331	−1 ± 7	1 ± 3	2 ± 3	−4 ± 3	0.04 ± 0.05	3.1	215
7626	1 ± 6	4 ± 3	−2 ± 2	−10 ± 2	0.38 ± 0.05	1.3	293
7742	−19 ± 11	−4 ± 4	−2 ± 3	−10 ± 5	0.59 ± 0.06	2.2	237

old-TOs, which have spatially uniform stellar populations, these gradients are not huge, with δ_V typically smaller than 0.5 mag. Young-TOs, with their diluted W_λ profiles, also have extinction gradients, but a quantitative assessment of their magnitude requires a more elaborate analysis, which we present in Section 4.2.2.

3.4 Slit profiles

The central intermediate age population, which dilutes the equivalent widths of metal lines, must cause an excess of flux with respect to the smooth surface brightness profile from the bulge of the host galaxy. Galaxies containing this extra central source should thus have sharper brightness profiles than those with more uniform stellar populations.

In order to verify this prediction we have measured the half width at half-maximum (HWHM) of the slit profiles, denoted by R_S. The results are listed in the last two columns of Table 2 in angular and linear scales, and graphically illustrated in Fig. 23. The plot confirms that the most compact slit profiles occur among sources with diluted $W_{\rm K}$ profiles. By extension of the relations between $\delta_{\rm K}$, $W_{\rm K}^{\rm nuc}$ and [O I]/Hα, one expects these compact sources to be mostly young-TOs, as confirmed in Figs 23(b) and (c).

The slit profiles of young-TOs suggests characteristic sizes of 50–100 pc for their central intermediate age population. This rough

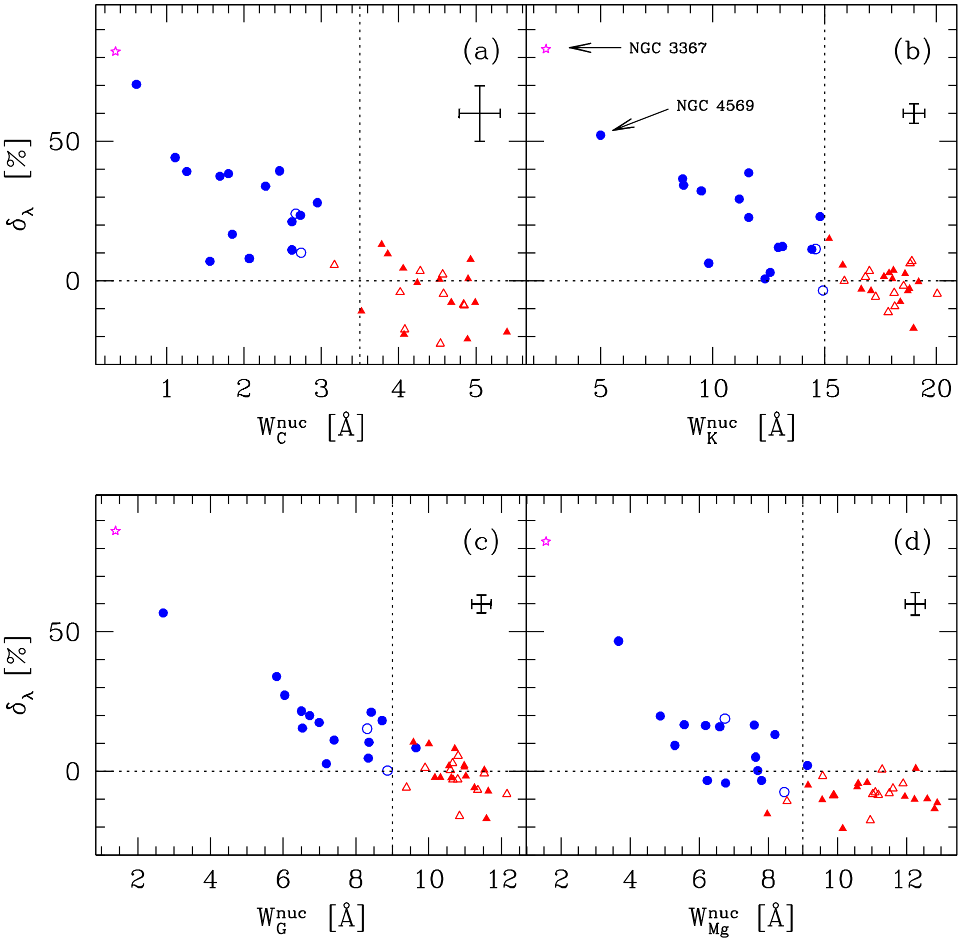

Figure 16. Radial gradients in four equivalent widths, measured from the comparison of nuclear and off-nuclear spectra. Different symbols correspond to young-TOs (filled blue circles), young-LINERs (open blue circles), old-TOs (filled red triangles) and old-LINERs (open red triangles). The star indicates the starburst galaxy NGC 3367. Crosses in the top right indicate mean error bars. Vertical dotted lines divide nuclei containing only old stars (large W_λ) from those with significant intermediate age populations (small W_λ). Note that NGC 6951, which has very negative δ_λ due to its star-forming ring, is outside all plot scales.

estimate suffers from two caveats. First, it is based on the total flux profile, which includes the bulge light. This issue is addressed in Section 4. Secondly, in several cases R_S corresponds to angular sizes of 1 arcsec or less (Table 2), in which case seeing starts to dominate size estimates. In fact, the comparison of galaxy and stellar profiles in the bottom panels of Figs 3–12 shows that while old-LLAGNs have spatially resolved profiles, in young-TOs the inner $S(r)$ profile is only marginally broader than the seeing disk, so R_S should be regarded as an upper limit for these objects. A more refined study of the inner morphology of LLAGNs based on high-resolution imaging is underway (González Delgado et al., in preparation).

4 ANALYSIS AND DISCUSSION

Our spatially resolved spectra of LLAGNs show that significant stellar population gradients occur almost exclusively in young-TOs. These gradients are caused mostly by an intermediate age population (0.1–1 Gyr), although in a few cases a <10-Myr nuclear starburst is also present (Papers I and II). The contribution of these stars to the total spectrum increases towards the nucleus, causing the radial dilution of metallic features. For consistence of notation, we hereafter denote this population the 'central young population' (CYP), where 'young' means $\lesssim$1 Gyr old.

In this section we present estimates of the physical size, luminosity and extinction of the CYPs in young-TOs. These estimates require separating the light from the CYP from that of older stars from the host's bulge, which in turn requires a more elaborate analysis than the eminently empirical description of gradients presented in the previous section. Two methods were developed with this purpose. We close this section with a discussion on what these CYPs looked like in the past and what they might evolve to.

4.1 Fits of the equivalent width profiles

A rough estimate of the size of the region responsible for the radial dilution of metal lines may be obtained by evaluating at which distance from the nucleus $W_K(r)$ crosses the dividing line at $W_K = 15$ Å, which characterizes the transition from 'young' to 'old' stellar populations in our simple classification scheme. This is not always possible, either because W_K sometimes does not rise above this threshold in the whole region analysed (e.g. NGC 4569; Fig. 10) or because of asymmetries or oscillations in the W_K profile (e.g.

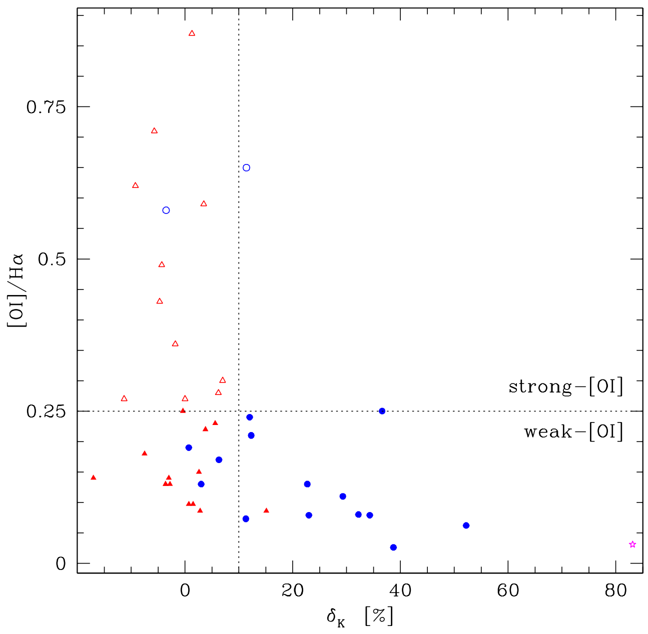

Figure 17. Radial dilution in the K line against the [O I]/Hα emission-line ratio (extracted from HFS97). Symbols as in Fig. 16. The horizontal line shows the [O I]/H$\alpha = 0.25$ taxonomical frontier which separates strong from weak [O I] nuclei. Objects to the right of the vertical line at δ_K = 10 per cent are those with significant dilution.

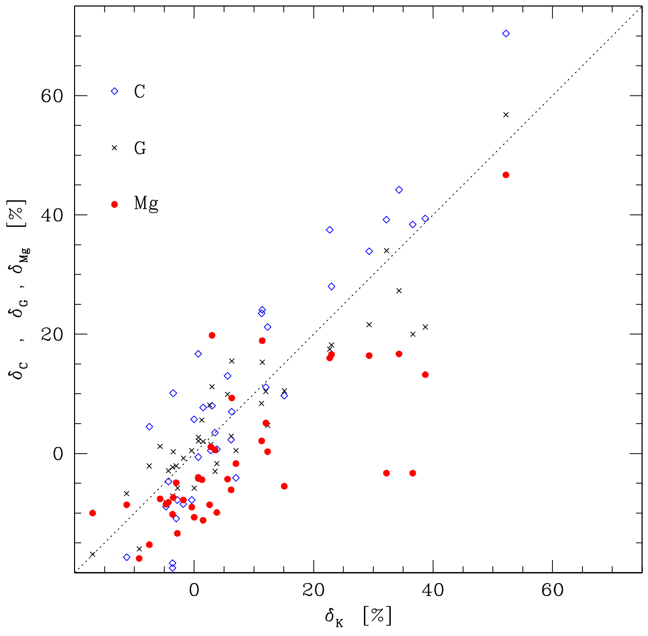

Figure 18. Dilution in W_C (diamonds), W_G (crosses) and W_{Mg} (filled circles) against the dilution in W_K. The diagonal line simply marks $y = x$. All sources in this plot are LLAGNs. Error bars have been omitted for clarity.

NGC 5678; Fig. 7). For the objects where this analysis was possible, we estimate radii between ∼100 and 300 pc.

A more formal estimate may be obtained by fitting the W_λ profiles. A two-component model was build for this purpose. We assume that $W_\lambda(r)$ results from the superposition of a 'background' component with a $W_\lambda(r) = W_\lambda(\infty)$ flat profile and a diluting component with negligible W_λ, and whose fractional contribution $f(r)$ to the total continuum at wavelength λ and position r follows a bell-shape radial distribution. The resulting model is expressed by

$$W_\lambda(r) = W_\lambda(\infty)\,[1 - f(r)] = W_\lambda(\infty)\left[1 - \frac{\Delta_\lambda}{1 + (r/a_W)^2}\right] \qquad (3)$$

where $\Delta_\lambda = [W_\lambda(\infty) - W_\lambda(0)]/W_\lambda(\infty)$ and $W_\lambda(\infty)$ are the analytical equivalents of δ_λ and $W_\lambda^{\rm off}$, respectively (see equation 1). a_W is the HWHM of the $f(r)$ profile, a size scale which should not be confused with the HWHM of the surface brightness profile associated with the central diluting component. The latter quantity, which we denote by R_W, must be evaluated from the product of $S(r)$ and $f(r)$.

We have fitted this model to the W_K profiles of 15 LLAGNs: NGC 404 and 4150, plus the 13 LLAGNs with $\delta_K > 10$ per cent (i.e. those with significant dilution). The results are reported in Table 3. The fits are generally good, as illustrated in Fig. 24. The dilution factors obtained from the fits are larger than those measured using equation (1), with $\Delta_K \sim 1.3\delta_K$ typically. This happens because in most cases our operational definition of $W_K^{\rm off}$ includes part of the rising portion of the $W_K(r)$ curve, while equation (3) fits an asymptotic value. Interestingly, we find $\Delta_K = 23$ and 29 per cent for NGC 404 and 4150, respectively, two young-TOs for which δ_K fails to detect significant dilution but, according to the qualitative considerations in Section 3.2, should be included in the list of sources with diluted W_K profiles.

The values of a_W range from ∼30 to 400 pc, with a median of 172 pc, in agreement with the cruder estimates based on the size of the $W_K < 15$ Å region. These values are larger than the HWHM of $S(r)$, which spans the $R_S = 20$–170 pc range, with a median of 93 pc for this subset of galaxies (Table 2). In other words, $f(r)$ is broader than $S(r)$. Therefore, in practice the HWHM of the light distribution associated with the CYP is dictated more by the slit profile than by the $f(r)$ deduced from the $W_K(r)$ fits. The $S \times f$ profiles yield $R_W = 17$ to 126 pc (median = 67 pc), just slightly smaller than R_S. Hence, although it is clear that these CYPs often extend to more than 100 pc from the centre (as demonstrated by the detection of HOBLs well outside the nucleus; e.g. Figs 1 and 2), most of their light is concentrated within $r \lesssim 100$ pc. The relatively little light from the outer ($r > R_W$) parts of this distribution is enough to compete with the flux from the host's bulge, producing diluted W_λ profiles on scales a_W substantially larger than R_W.

It is important to emphasize that, in angular units, the median R_W corresponds to just 0.8 arcsec. Hence, although we are able to resolve the wings of the light profile of CYPs, seeing prevents us from adequately sampling their core. Our estimates of R_W should thus be regarded as upper limits to the actual CYP radius. Indeed, high-resolution images of a few young-TOs reveal structures on scales smaller than those we are able to trace with our ∼1-arcsec resolution. For example, NGC 4569 is known to have a very strong and compact nuclear source. Maoz et al. (1996) found, based on an *HST* Faint Object Camera image at 2300 Å, that the emission of this galaxy is composed of a bright unresolved nuclear point source and some faint extended emission 0.65 arcsec south of the nucleus. Similar observations by Barth et al. (1998), made with the *HST* Wide Field Planetary Camera 2 at 2200 Å, find that the nucleus is slightly resolved along PA = 20°, with a dimension of 0.16 × 0.11 arcsec^2.

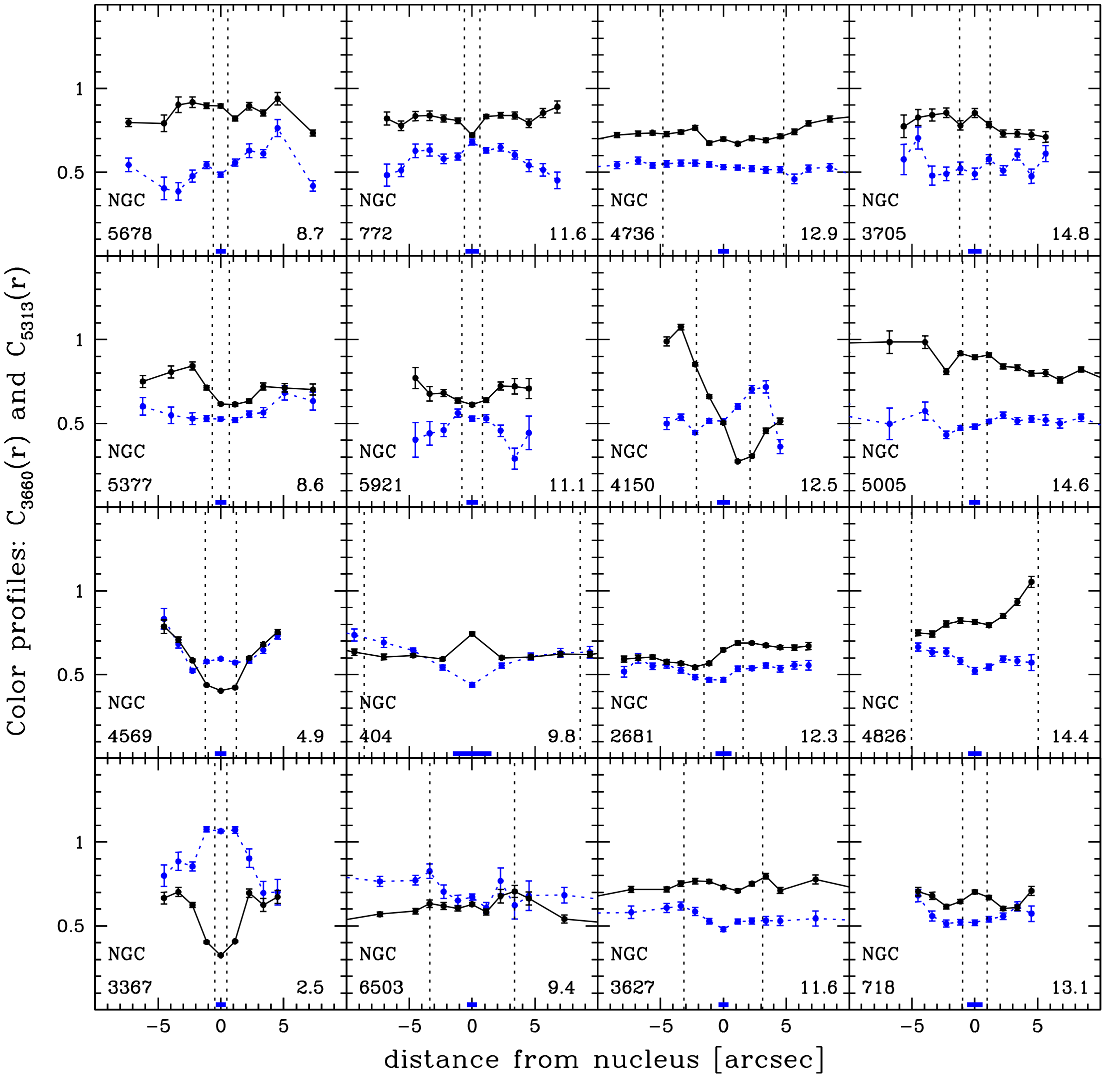

Figure 19. Radial profiles of two continuum colours: $C_{3660} = 3660/4020$ (dotted, blue line) and 5313/4020 (solid, black line). Note that the values of C_{5313} have been divided by 2 for plotting purposes. Dotted vertical lines mark distances of ±100 pc from the nucleus. Objects are sorted by the value of $W_{\rm K}$ at the nucleus, indicated in the bottom-right corner of each panel. Galaxies in this figure have $W_{\rm K}^{\rm nuc}$ between 2.5 (bottom left-hand panel) and 14.8 Å (top right).

4.2 Template decomposition

4.2.1 *Method*

An alternative and more complete way to analyse gradients in stellar populations is to model each extraction in terms of a superposition of spectra of well-understood stellar populations. This can be achieved by means of the empirical starlight modelling scheme introduced in Paper I. The method consists of fitting a given spectrum with a combination of five non-active galaxies from our comparison sample, whose spectra represent stellar population classes $\eta =$ Y (NGC 3367), I (NGC 205), I/O and O (NGC 221, 1023 and 2950). The code outputs the fractional contribution of these components to the flux at 4020 Å, expressed as a population vector $\boldsymbol{x} = (x_{\rm Y}, x_{\rm I}, x_{\rm O})$, where the $\eta =$ I/O and O components are grouped in $x_{\rm O}$ for conciseness. The code also fits the extinction A_V, modelled as due to an uniform dust screen with A_V up to 4 mag. Regions around emission lines are masked out in the comparison of model and observed spectra. Paper I shows that this method provides excellent fits to the spectra. Unlike in Papers I and II, we have dereddened the template galaxies by their intrinsic extinction derived by method described in Cid Fernandes et al. (2004b). Only NGC 3367 and 205 are found to have significant extinction, both with $A_V \sim 0.9$ mag. These corrections were applied because of our interest in estimating the extinction and its radial variations in LLAGNs.

We have applied this method to all nuclear and off-nuclear spectra analysed in this paper, thereby producing stellar population and extinction profiles. The spectral fits are of similar quality to those exemplified in Paper I. The median fractional difference between model and observed spectra for all extractions is 4.5 per cent, which is acceptable considering a median S/N ratio of 6 per cent at 4000 Å and 3 per cent at 4800 Å.

Examples of the resulting $\boldsymbol{x}(r)$ and $A_V(r)$ are illustrated in Fig. 25. The population vector in these plots is grouped into a predominantly old component, $x_{\rm O}$ (dotted red line), and a young plus intermediate age component, $x_{\rm Y+I} = x_{\rm Y} + x_{\rm I}$ (solid blue line), representing the combined strengths of the NGC 3367- and 205-like components. This coarse two-component description of the stellar population matches our young/old classification scheme. The $x_{\rm Y+I}(r)$ fraction, in particular, is used to map the CYP. We further plot $x_{\rm Y}(r)$ as a

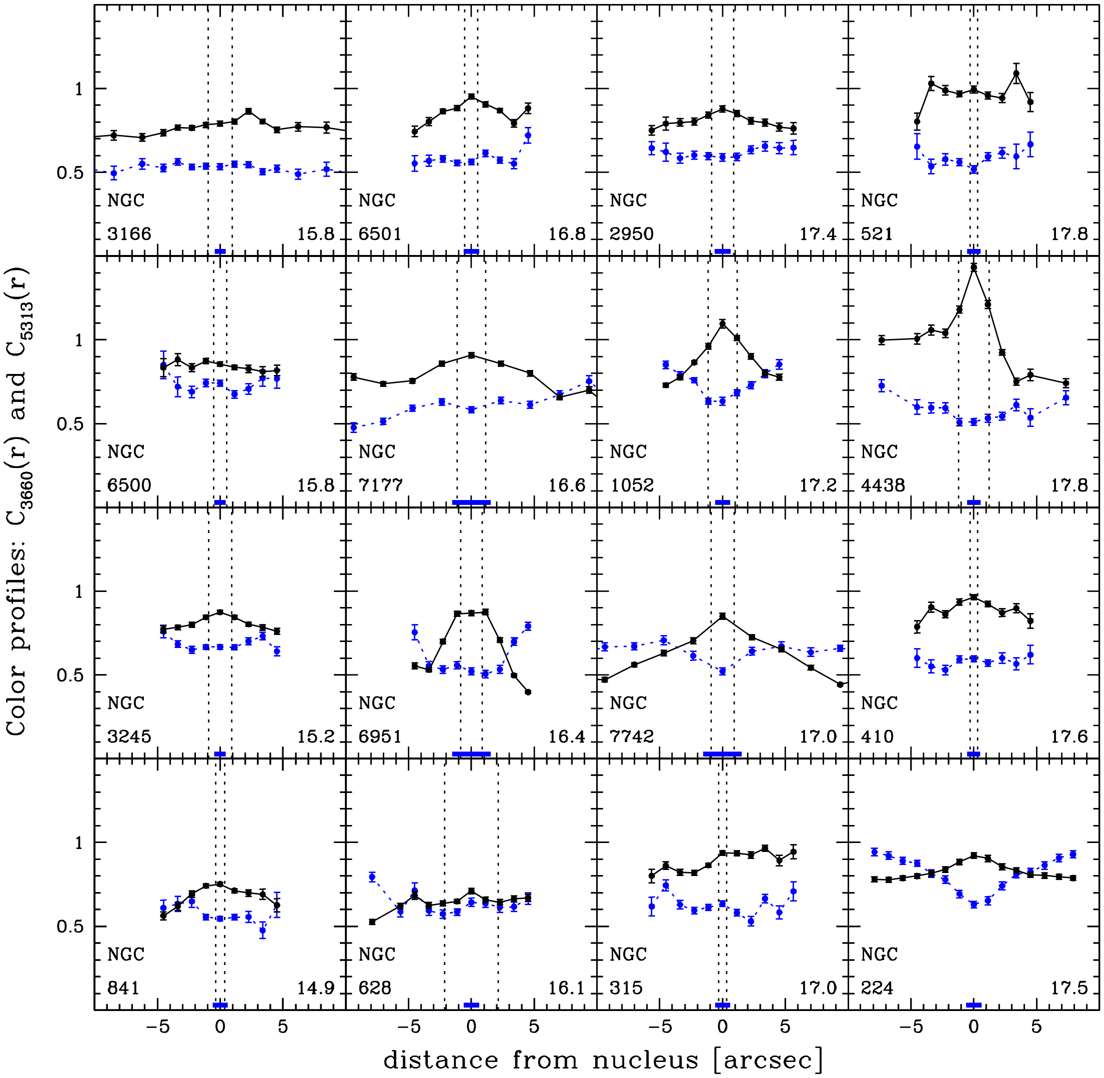

Figure 20. As Fig. 19, but for galaxies with $W_{\mathrm{K}}^{\mathrm{nuc}}$ between 14.9 and 17.8 Å.

dashed line to illustrate that $x_{\mathrm{Y+I}}$ is actually dominated by the intermediate age population. As found in Papers I and II, young starbursts are generally weak or absent in LLAGNs, although off-nuclear star formation occurs in a few cases, as in NGC 6951. This old-TO provides a good example of the power of the method (Fig. 25c). Its well-known star-forming ring (Pérez et al. 2000), at $r \sim 4$ arcsec $\sim$500 pc, is nicely mapped by the $x_{\mathrm{Y+I}}$ profile and its associated brightness distribution (bottom panel), obtained from the multiplication of $x_{\mathrm{Y+I}}(r)$ by the slit profile $S(r)$. Notice also the rise in extinction in the ring, the presence of an intermediate age component throughout the observed region, particularly in the ring, and the prevalence of an old, bulge-like population in the nucleus, which accounts for over 70 per cent of the light.

Fig. 26 shows the $\boldsymbol{x}(r)$ profiles for all 42 LLAGNs in our sample. As in previous plots, galaxies are ordered from bottom right to top left in an increasing sequence of $W_{\mathrm{K}}^{\mathrm{nuc}}$. The plot confirms that the spectral gradients identified in Section 3 are indeed associated with a centrally concentrated intermediate age stellar population, plus, in a few cases, a young starburst (e.g. NGC 772). This can be seen by the peaked $x_{\mathrm{Y+I}}$ profiles from NGC 4569 to 6500 in Fig. 26. Conversely, the old stellar component, mapped by $x_{\mathrm{O}}(r)$ in these plots, bears a clear similarity in shape with the W_λ profiles: galaxies with diluted lines have diluted $x_{\mathrm{O}}(r)$ profiles. Similarly, the spatial homogeneity of stellar populations inferred from the flat $W_\lambda(r)$ in galaxies such as NGC 266 and most others in the right half of Fig. 26 is confirmed by equally flat x_{O} profiles, while peaked W_λ profiles map on to peaked x_{O} profiles (e.g. NGC 1161).

Hence, to first order, the $\boldsymbol{x}(r)$ profiles obtained from the template decomposition merely map the W_λ variations on to the stellar population space spanned by our normal galaxy base. In fact, this relation is so strong that the equation

$$x_{\mathrm{O}} = (0.068 \pm 0.001) W_{\mathrm{K}}\,[\text{Å}] - (0.35 \pm 0.02) \tag{4}$$

transforms W_{K} into x_{O} to within better than 0.1 rms for all 521 spectra. Putting our $W_{\mathrm{K}}^{\mathrm{nuc}} = 15$ Å dividing line in this equation, we find that the transition from young to old stellar population occurs around $x_{\mathrm{O}} \sim 2/3$, or, equivalently, $x_{\mathrm{Y+I}} \sim 1/3$. We thus conclude that CYPs which account for $\lesssim$1/3 of the optical light would not be recognized as such in our data. Indeed, of the 15 LLAGNs with CYPs detected through the radial dilution of W_{K}, only two have $x_{\mathrm{Y+I}} < 1/3$: NGC 4826 ($W_{\mathrm{K}}^{\mathrm{nuc}} = 14.4$ Å and $x_{\mathrm{Y+I}} = 0.25$) and NGC 3245 ($W_{\mathrm{K}}^{\mathrm{nuc}} = 15.2$ Å and $x_{\mathrm{Y+I}} = 0.23$).

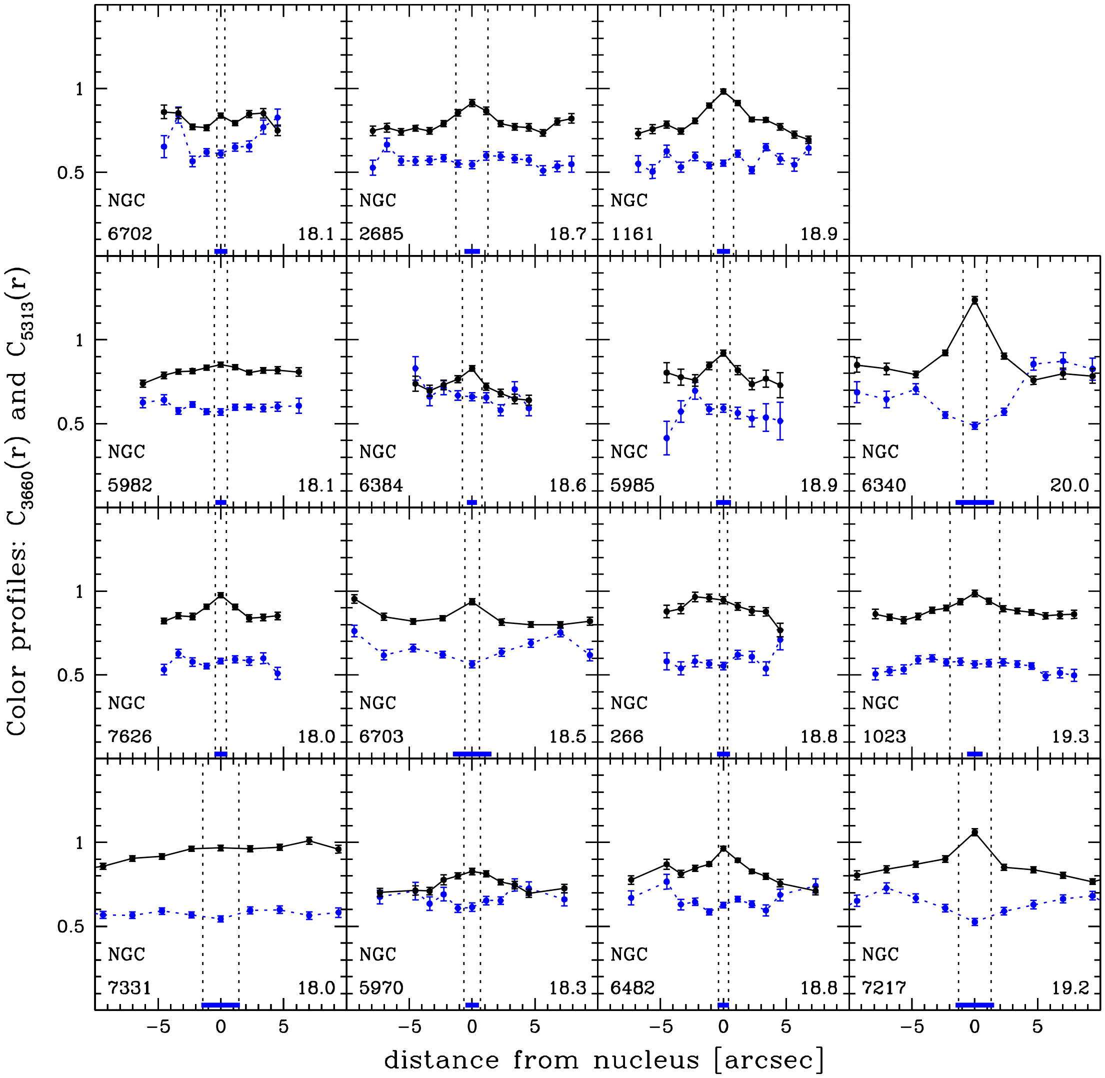

Figure 21. As Fig. 19, but for galaxies with $W_{\rm K}^{\rm nuc}$ between 18 and 20 Å.

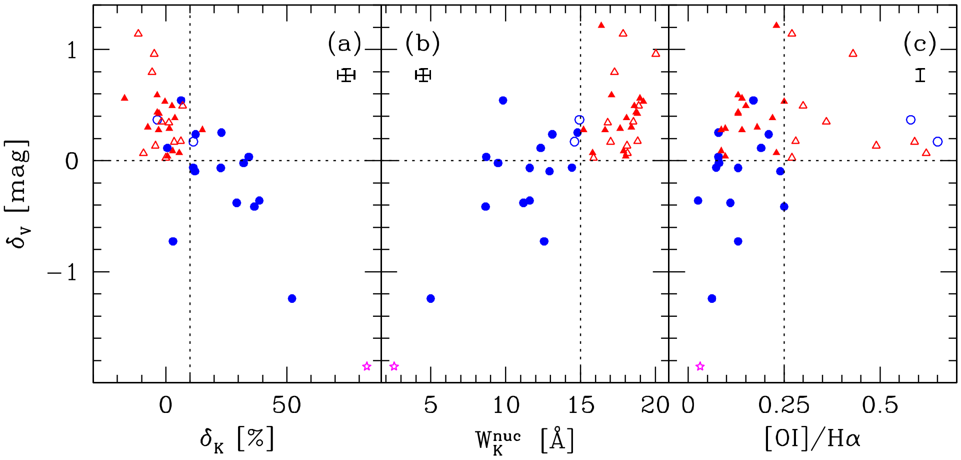

Figure 22. Colour gradients, as given by the differential extinction δ_V implied by the 5313/4020 colour, plotted against (a) the dilution in the K line, (b) the nuclear equivalent width of the K line, and (c) [O I]/Hα. Nuclei which are redder (bluer) than the off-nuclear spectra have positive (negative) δ_V. Symbols as in Fig. 16.

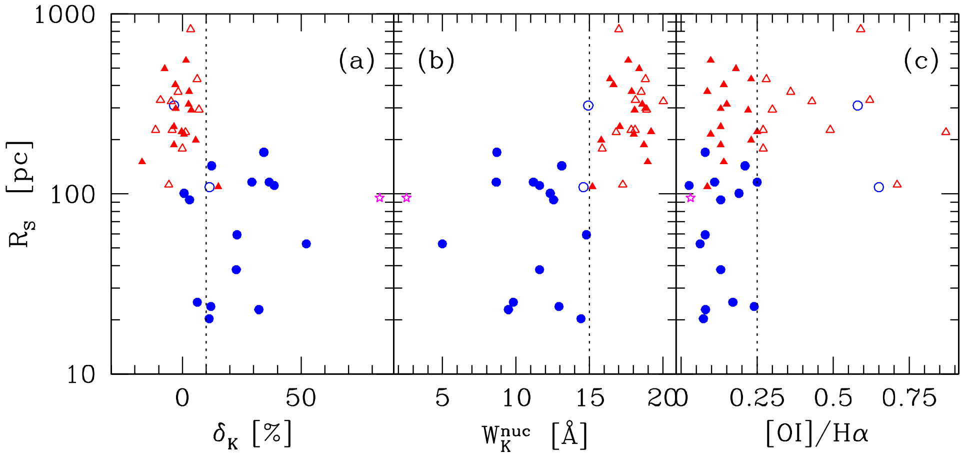

Figure 23. HWHM of the flux distribution along the slit plotted against (a) the dilution in the K line, (b) the nuclear equivalent width of the K line, and (c) [O I]/Hα. Symbols as in Fig. 16.

Table 3. Results of the $W_{\rm K}(r)$ fits for LLAGNs with diluted $W_{\rm K}$ profiles.

NGC (1)	$W_{\rm K}(\infty)$ (Å) (2)	$\Delta_{\rm K}$ (per cent) (3)	a_W (arcsec) (4)	a_W (pc) (5)	R_W (arcsec) (6)	R_W (pc) (7)
0404	12.2 ± 0.4	23 ± 4	3.7 ± 0.5	43 ± 6	1.7 ± 0.1	20 ± 1
0718	17.9 ± 1.4	28 ± 6	3.6 ± 0.6	374 ± 65	1.2 ± 0.1	126 ± 5
0772	19.9 ± 0.3	42 ± 3	1.1 ± 0.1	172 ± 20	0.5 ± 0.1	86 ± 3
3245	18.2 ± 0.3	17 ± 2	1.0 ± 0.3	107 ± 29	0.6 ± 0.1	67 ± 8
3627	15.5 ± 0.3	25 ± 3	1.4 ± 0.3	44 ± 9	0.8 ± 0.1	25 ± 2
3705	20.4 ± 0.7	28 ± 4	1.7 ± 0.5	139 ± 39	0.6 ± 0.1	52 ± 3
4150	15.7 ± 1.3	29 ± 7	4.2 ± 0.7	199 ± 32	1.8 ± 0.1	82 ± 3
4569	22.6 ± 2.4	78 ± 2	4.5 ± 0.5	365 ± 37	0.6 ± 0.1	52 ± 3
4736	15.6 ± 0.2	17 ± 2	2.3 ± 0.6	47 ± 12	0.9 ± 0.1	19 ± 1
4826	17.0 ± 0.6	15 ± 4	2.0 ± 0.7	39 ± 14	0.8 ± 0.1	17 ± 2
5005	16.5 ± 0.3	15 ± 3	1.7 ± 0.2	172 ± 24	0.8 ± 0.1	85 ± 4
5377	18.6 ± 1.0	52 ± 2	2.6 ± 0.4	388 ± 59	0.7 ± 0.1	106 ± 2
5678	13.2 ± 0.7	33 ± 4	1.1 ± 0.7	190 ± 115	0.6 ± 0.2	110 ± 34
5921	18.2 ± 1.7	38 ± 6	2.0 ± 0.5	244 ± 63	0.8 ± 0.1	96 ± 7
6503	14.4 ± 0.6	34 ± 4	1.1 ± 0.4	31 ± 13	0.6 ± 0.1	17 ± 3

4.2.2 Extinction profiles

Our empirical analysis of colour and equivalent width gradients in Section 3.3 indicates that extinction gradients are generally small in old-LLAGNs, while for young systems we could only reach the qualitative conclusion that extinction variations must occur. A much more refined analysis is possible with the template decomposition method, which produces quantitative estimates of both gradients and absolute values of the extinction.

The $A_V(r)$ profiles derived by this method are presented in Fig. 27 for our 42 LLAGNs. The first result which strikes the eye in this plot is the obvious asymmetry between galaxies in the left and right halves of the figure, which, given the ordering according to $W_{\rm K}^{\rm nuc}$, essentially correspond to young and old systems, respectively. The extinction profiles of young-LLAGNs are substantially more complex than those of old-LLAGNs, which are often approximately flat. In both cases, extinction gradients, when present, are generally in the sense of producing centrally peaked A_V profiles, indicating a higher concentration of dust in the central regions. It is nevertheless clear that other types of dust distribution exist, as in NGC 4150 and 4826, whose asymmetric $A_V(r)$ curves indicate the presence of off-nuclear dust lanes.

A second and even more obvious result from Fig. 27 is that there is a clear offset in the absolute values of A_V between young and old systems. The statistics of A_V reflect this difference. Averaging $A_V(r)$ over all extractions for each galaxy, we obtain a median spatially averaged extinction of 0.42 for our 16 young-LLAGNs, compared to 0.11 for the 26 old-LLAGNs. A similar offset is found considering only the nuclear extractions, which have median $A_V(0) = 0.62$ and 0.21, respectively. Young-LLAGNs, $\sim$90 per cent of which are young-TOs, are therefore $\sim$ three times dustier than old-LLAGNs. The clearest exception to this strong correlation is NGC 4438. The high concentration of dust inferred from the A_V profile of this old-LINER is associated with the pronounced nuclear dust lane seen in *HST* images (Kenney & Yale 2002).

The Balmer decrement measurements of HFS97 lend further support to interpretation that young-TOs have a higher dust content than other LLAGNs. Using their tabulated values for objects in our sample, we find a median Hα/Hβ of 4.6 for young-TOs and 3.1 for other LLAGNs. We can extend this analysis to the whole HFS97 sample using their measurements of the G-band equivalent width and classifying LLAGNs into young or old adopting a W(G-band) = 4 Å dividing line, which is roughly equivalent to our young/old division at $W_{\rm K} = 15$ Å (Paper I). The 27 young-TOs in this larger sample have a median Hα/Hβ = 4.5, while for the other 116 LLAGNs this ratio is 3.2.

We thus conclude that all evidence points towards a scenario where young-TOs are the dustier members of the LLAGN family.

4.2.3 Sizes and luminosities of the CYPs

The population vector derived through the template decomposition analysis may be combined with the slit profiles to produce one-dimensional surface brightness profiles of the different stellar populations in our galaxies, as illustrated in the bottom panels of Fig. 25. In what follows we use this method to estimate sizes and luminosities of the CYPs, represented by the $S_{\rm CYP}(r) = S(r) \times x_{\rm Y+I}(r)$ profile. This method differs from that in Section 4.1 in two aspects: (i) instead of assuming a functional form for the light fraction associated with the CYP, we derive this fraction empirically from the template decomposition; (ii) all the spectrum is used, as opposed to a single equivalent width.

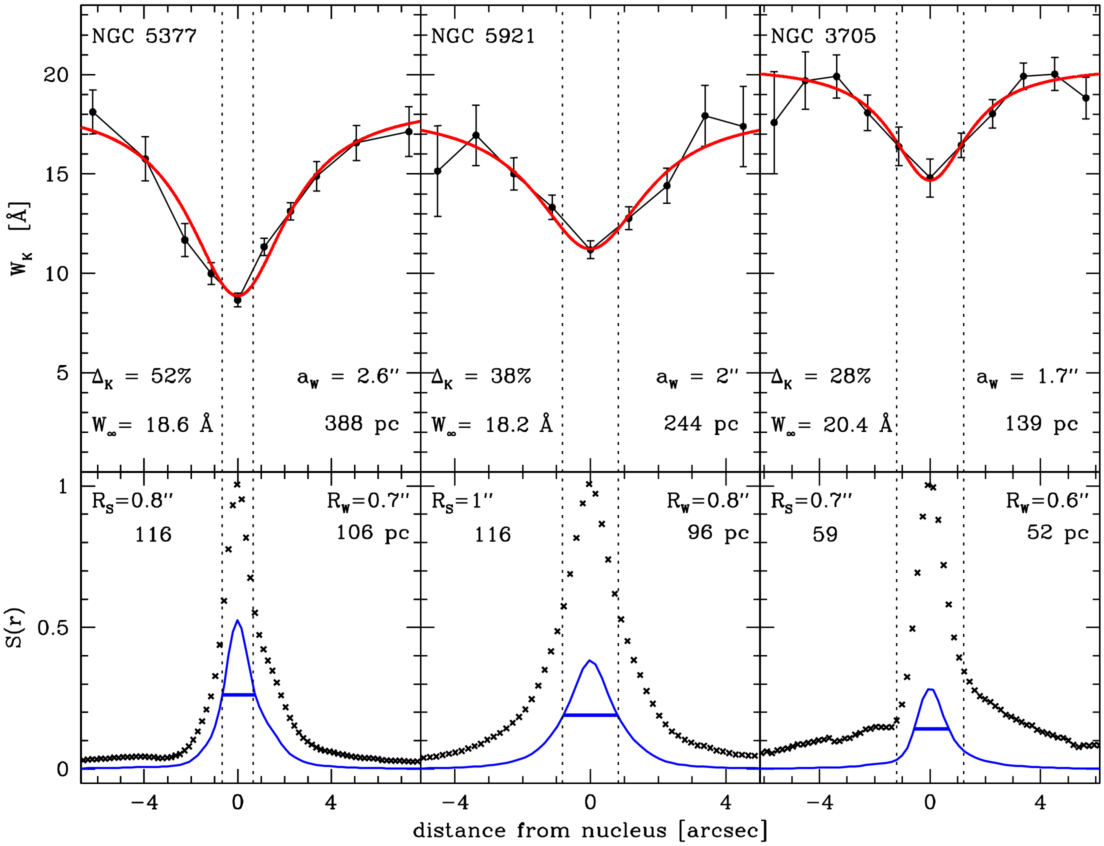

Figure 24. Top: examples of the $W_{\rm K}(r)$ fits. Bottom: crosses show the normalized slit brightness profile. The solid blue line shows the brightness profile of the diluting component inferred from the $W_{\rm K}(r)$ fits. Labels indicate the HWHM of the total brightness profile (R_S) and the HWHM of the diluting source (R_W), also indicated by the thick horizontal line segment. Vertical dotted lines mark projected distances of ±100 pc from the nucleus.

Fig. 28 shows the total slit profile $S(r)$ (thin black line), and its decomposition into young (thick blue line) and old (dotted red) components for our 42 LLAGNs. The plot shows that the young components dominate the light in the inner ∼100 pc from NGC 4569 up to 718 ($W_{\rm K}^{\rm nuc} = 13.1$ Å), becoming fainter than the inner old population as $W_{\rm K}^{\rm nuc}$ increases, until it eventually 'vanishes' from NGC 7177 onwards ($W_{\rm K}^{\rm nuc} > 16.6$ Å). Note that, unlike all other profiles in this paper, Fig. 28 uses a linear scale for r, which emphasizes the compactness of the CYPs in young-TOs.

We estimate the radius of the CYPs from the HWHM of the $S_{\rm CYP}(r)$ profiles. Table 4 presents our results. As for the $W_{\rm K}(r)$ fits, we obtain $x_{\rm Y+I}$ profiles which are broader than $S(r)$, so $R_{\rm CYP}$ is close to R_S (Table 2). The values of $R_{\rm CYP}$ are in good agreement with R_W (Table 3), which is the equivalent CYP radius in the $W_{\rm K}(r)$ fits. Again, these estimates should be regarded as upper limits, given that the angular sizes are limited by our spatial resolution.

The luminosity associated with the CYPs was estimated integrating $S_{\rm CYP}(r)$ within $|r| < 5\ R_S$. The integration is performed in half-rings of area $\pi r\ {\rm d}r$, i.e. extrapolating our one-dimensional profiles to two dimensions. Table 4 lists both the total and CYP luminosities. Numbers in parentheses correspond to luminosities corrected by intrinsic extinction using the modelled A_V profiles. The resulting dereddened CYP luminosities at 4020 Å range from $L_{\rm CYP} \sim 10^{3.3}$ to $10^{5.5}$ $L_\odot$ Å^{-1}, with a median of $10^{4.3}$ $L_\odot$ Å^{-1}. Expressed in more conventional units, this roughly corresponds to a range in B-band absolute magnitudes[1] from ~ -12.2 to -17.7, with a median $M_B = -14.7$. Given the uncertainties in absolute flux calibration, extinction correction and extrapolation from one-dimensional to two-dimensional profiles, these values should be taken as order of magnitude estimates. Yet, they are precise enough for the general considerations we present next.

4.3 Discussion: the past and future of young-TOs

Naturally, the intermediate age stars which typify the CYPs of young-TOs have been younger in the past and will become older in the future. Their current age and luminosity can be used, with the aid of evolutionary synthesis models, to predict what these objects looked like in their early days and what they will eventually become.

For simplicity, let us assume that CYPs formed in instantaneous bursts 10^8–10^9 yr ago. From the Starburst99 models of Leitherer et al. (1999) we infer that these CYPs were ∼10 to 100 times more luminous in the optical in their first few Myr of life. Because the old stellar population has not changed substantially over this period, the CYPs would be much easier to detect back then. The weakest CYPs recognized as such in our sample (i.e. those with $W_{\rm K}^{\rm nuc} \leqslant 15$ Å) presently account for $x_{\rm Y+I} \sim 33$ per cent of the nuclear light at λ4020. Scaling their present luminosity by factors of 10–100 would raise this fraction to 83–98 per cent, which shows that they would completely outshine the bulge light, and the optical continuum would be essentially identical to that of a starburst galaxy. Recall, however, that young-TOs are dusty, so these luminous infant CYPs could be substantially reddened and thus powerful far-infrared sources, particularly if they had even more dust (and gas) in their early phases.

---

[1] We use an $M_B \approx -2.5 \log L_{4020} - 3.96$ conversion, for L_{4020} in units of $L_\odot$ Å^{-1}, derived from the Starburst99 models.

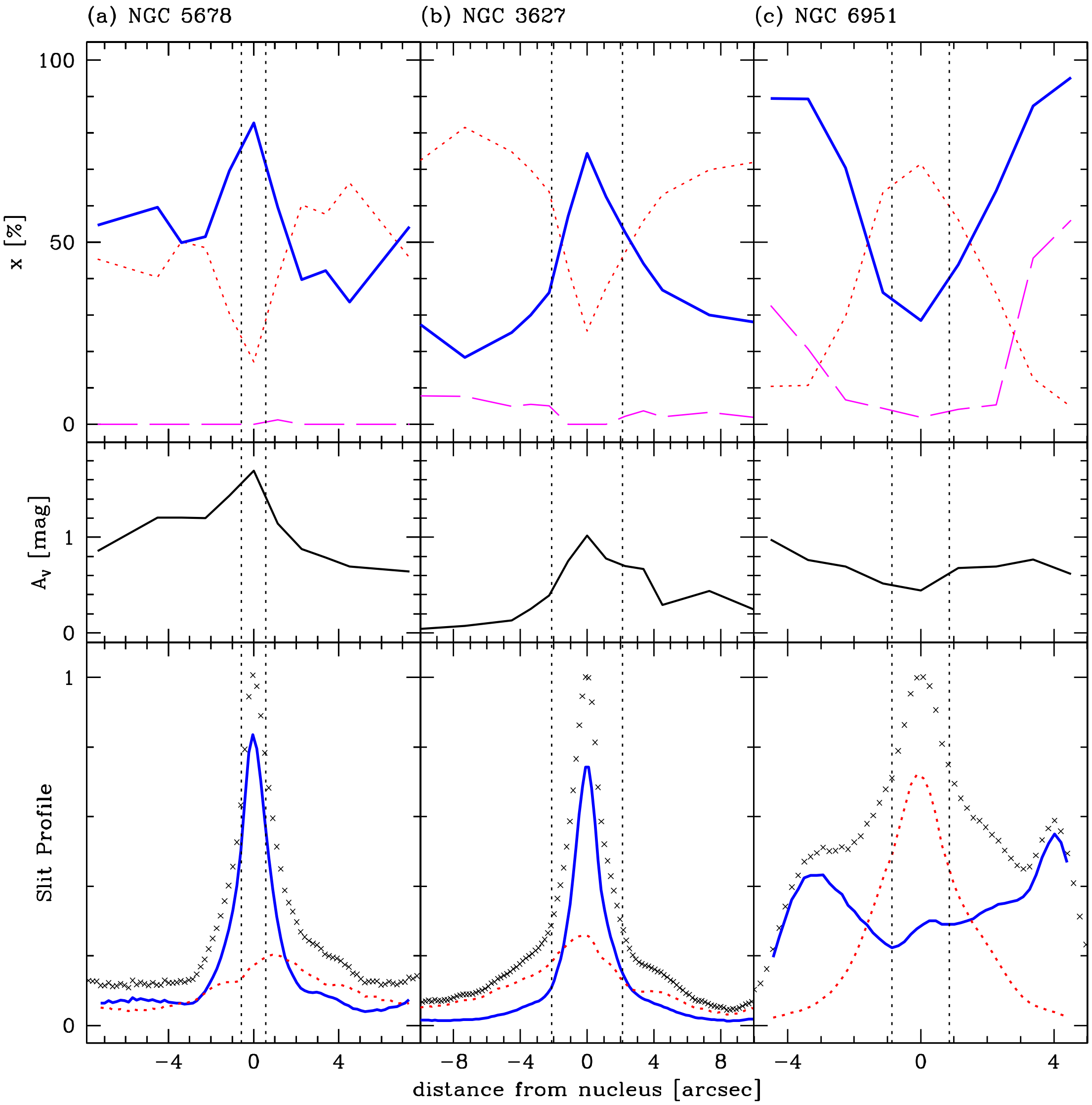

Figure 25. Examples of the results of the spectral fit of the spatially resolved spectra of three LLAGNs using a base of template galaxies. Top: radial profile of the population vector. Old stellar populations ($x_{\rm I/O} + x_{\rm O}$) are represented by dotted (red) lines, young plus intermediate and age populations ($x_{\rm Y+I} = x_{\rm Y} + x_{\rm I}$) by a solid (blue) line and young starbursts ($x_{\rm Y}$) by a dashed line. Middle: radial profile of the extinction $A_V(r)$. Bottom: crosses show the observed surface brightness profile along the slit, normalized to its peak value. The solid (blue) and dotted (red) lines represent the profiles associated with the young plus intermediate and old components, respectively. Vertical dotted lines indicate projected distances of ±100 pc from the nucleus.

The hot, massive stars in these early phases would have a large impact in the ionizing photon field. The Hα to λ4020 flux ratio for young starbursts is of the order of 1000 Å (Leitherer et al. 1999). Currently, CYPs have $L_{\lambda 4020} \sim 10^{4.3}$ L$_\odot$ Å^{-1} (Table 4), which scaled back to $t = 0$ yields Hα luminosities of the order of 10^{42} erg s^{-1}, more than two orders of magnitude larger than those currently observed in young-TOs and LLAGNs in general, which range from 10^{38} to 10^{40} erg s^{-1} (HFS97). In terms of $L_{H\alpha}$, they would rank among powerful starburst nuclei and Seyferts. Clearly, these objects would definitely not be classified as 'low luminosity' in their youth. It is not clear whether they would be classified as AGNs either. Unless the AGN too was much brighter in the past, these objects would surely look like starbursts

Simple stellar populations of ages between $t \sim 10^8$ and 10^9 yr have mass-to-light ratios at λ4020 of ∼500–5000 M$_\odot$ L$_\odot^{-1}$ Å in the solar metallicity models of Bruzual & Charlot (2003). For a median CYP luminosity of $10^{4.3}$ L$_\odot$ Å^{-1} (Table 4), this implies CYP masses $M_{\rm CYP} \sim 10^7$–10^8 M$_\odot$. Star formation has either ceased long ago or proceeds at a residual level in CYPs, otherwise they would look much younger. It is thus reasonable to suppose that these stars formed over a period of time whose length is a fraction of their current age. For star formation time-scales of 10^7–10^8 yr, the typical star formation rate was of the order of 1 M$_\odot$ yr^{-1}. These are clearly very rough estimates, but they serve to set the scale of the CYP phenomenon.

The precursors of young-TOs thus have to be luminous nuclei with substantial amounts of star formation and possibly a bright AGN too. Another clue is that these precursors must be found in the local Universe, because $t \leqslant 10^9$ yr corresponds to $z < 0.1$ for any reasonable cosmology. Two plausible contenders for the progenitors of young-TOs are starburst nuclei and starburst plus Seyfert 2 composites such as Mrk 477, Mrk 1210 and others (Heckman

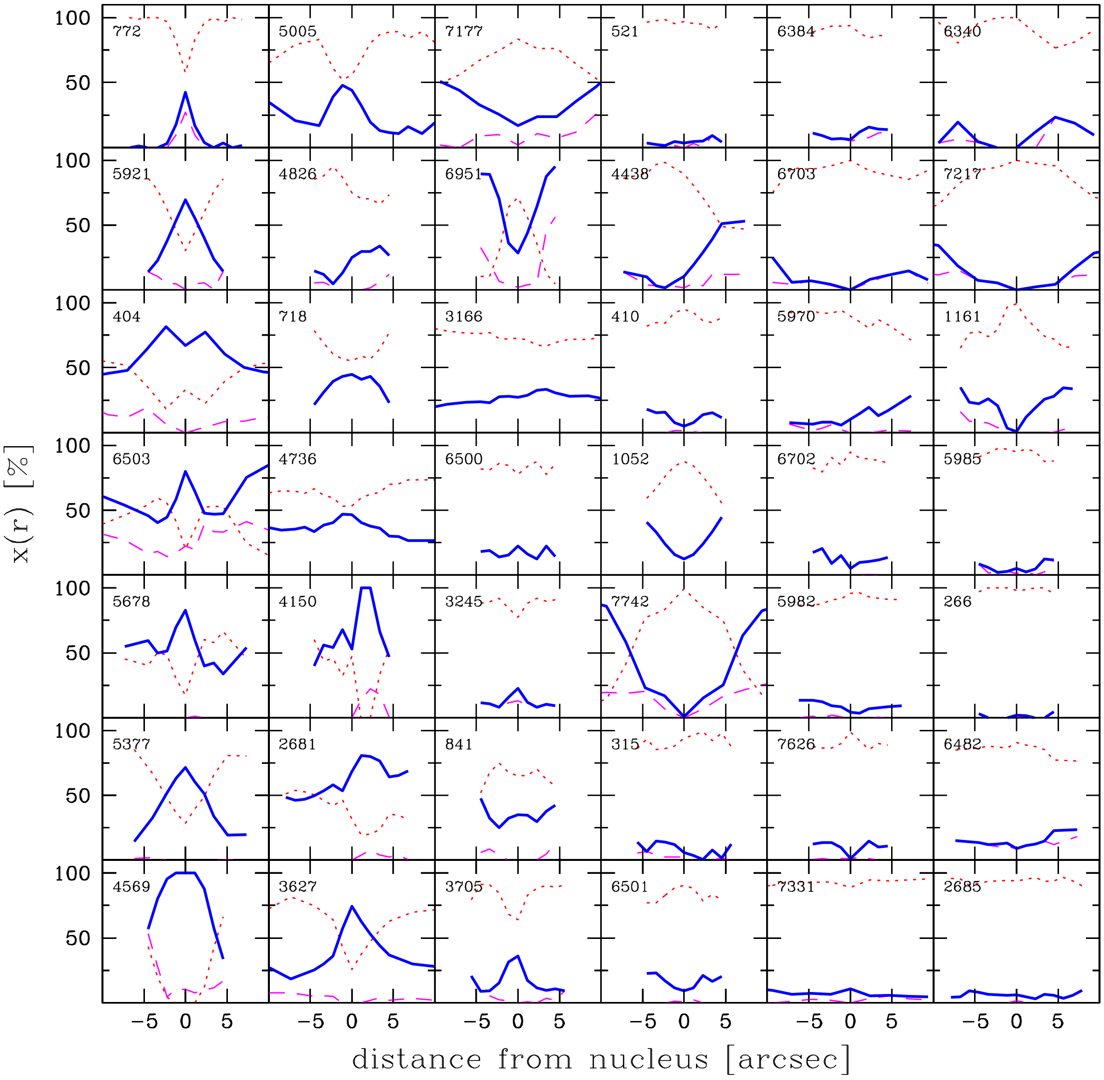

Figure 26. Results of the template decomposition for all 42 LLAGNs. Plots are ordered according to the value of $W_{\rm K}^{\rm nuc}$, from small values in the bottom left to large values in the top right. Dotted red lines correspond to $x_{\rm O}$, solid blue lines correspond to $x_{\rm Y+I}$ and dashed lines to $x_{\rm Y}$.

et al. 1997; Storchi-Bergmann et al. 1998; González Delgado et al. 2001). Given the tendency of TOs to have later Hubble types than LINERs and Seyferts (Ho, Filippenko & Sargent 2003), it seems more attractive to link young-TOs with starburst nuclei. However, the substantial overlap in morphological properties between TOs and both starburst and AGN hosts, coupled to indications that starburst plus Seyfert 2 composites have rather late-type morphologies for AGNs (Storchi-Bergmann et al. 2001), prevents us from drawing a firm conclusion at this stage.

Similar arguments can be used to sketch the future evolution of young-TOs. As the CYP fades, it will eventually cross the $x_{\rm Y+I} = 1/3$ threshold below which we would no longer identify it and the system would be classified as old (Section 4.2.1). For instance, starting from a current value of $x_{\rm Y+I} = 2/3$, and assuming the old population does not change much, the CYP would cross the $x_{\rm Y+I} = 1/3$ line after it fades by a factor of 4. For an assumed age of 1 Gyr, this would take ∼2 Gyr to occur. In other words, the stellar populations of young-TOs will become indistinguishable from those of old-LLAGNs in a few Gyr. Although it is tempting to link young-TOs to old-TOs because of their identical emission-line properties, as pointed out in Paper II we cannot rule out the possibility that [O I]/Hα increases as the CYP fades, which would turn a young-TO into an old-LINER. Note also that for either of these two evolutionary connections to work, young-TOs must some how get rid of their excess dust (Section 4.2.2) in a few Gyr, either by converting it to new stars or blowing it away.

Although much work remains to be done, these general considerations illustrate how the careful dissection of stellar population properties can provide new and important pieces in the quest to solve the puzzle of AGNs. The evolutionary scenarios sketched above will be examined more closely in forthcoming communications.

5 CONCLUSIONS

In this third paper in our series dedicated to the stellar populations of LLAGNs, we have investigated the radial variations of stellar population properties in a sample of 42 LINERs and TOs plus five non-active galaxies. The analysis was based on high-quality 3500–5500 Å long-slit spectra covering angular regions of at least ∼10 arcsec in diameter with a resolution of ∼1 arcsec (corresponding to ∼100 pc).

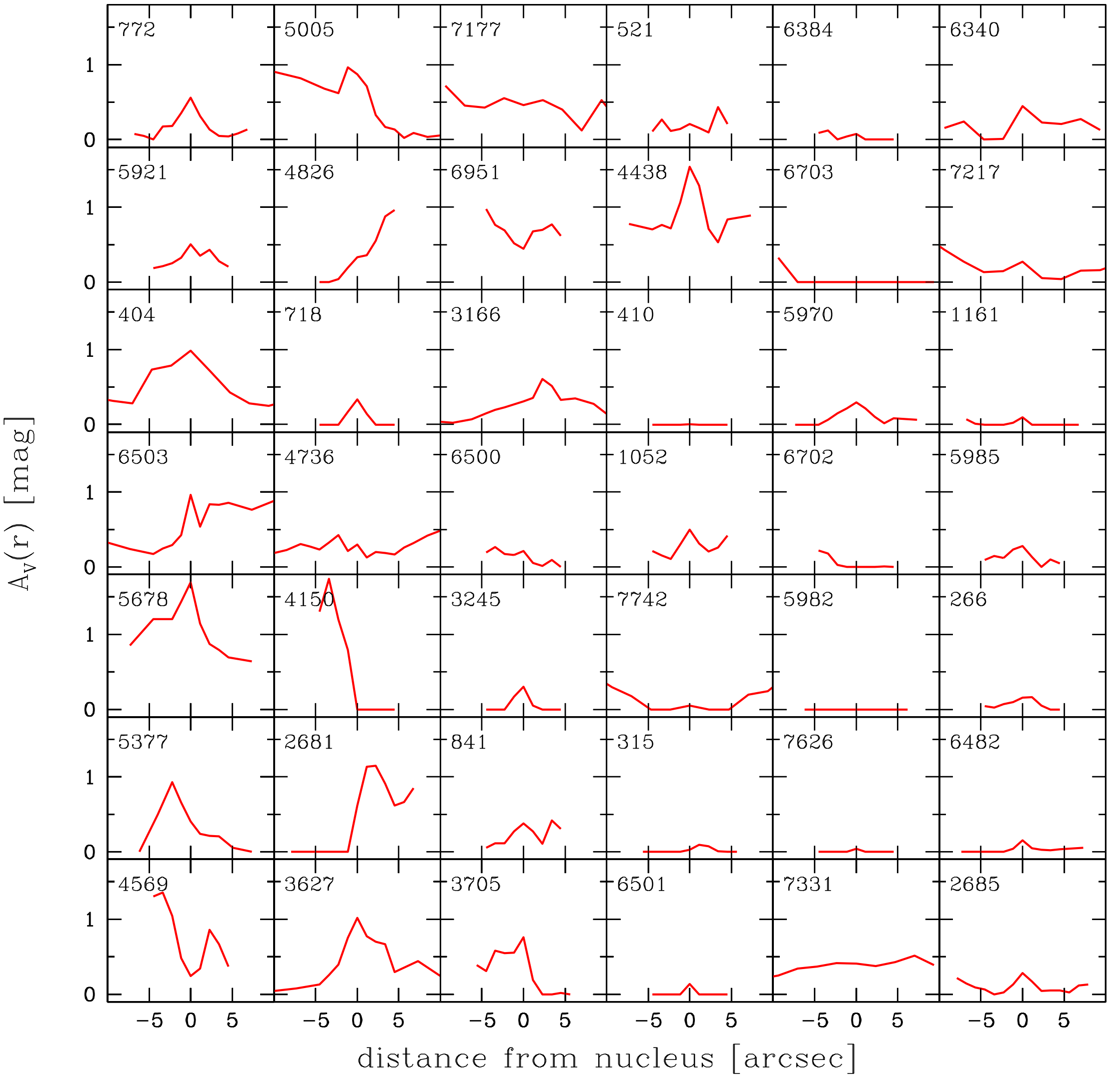

Figure 27. Extinction profiles obtained from the template decomposition analysis. The ordering of the galaxies is as in Fig. 26.

The main result of Papers I and II was the identification of a class of objects which stand apart from other LLAGNs in having a strong 10^{8-9} yr population. In terms of emission lines, nearly all of these nuclei have weak [O I]/Hα, hence their denomination as 'young-TOs'. Here we have shown that young-TOs are also distinct from other LLAGNs in terms of the way stellar populations and dust are spatially distributed. This general conclusion was reached through two distinct and complementary ways.

First, radial profiles of absorption-line equivalent widths, continuum colours and the total flux along the slit were used to trace the spatial distribution of stellar populations. The results of this empirical analysis can be summarized as follows.

(i) We find that the W_λ profiles are of essentially two types: flat and diluted. Flat profiles, which indicate spatially uniform stellar populations, are more common, accounting for ~60 per cent of the sample. They occur exclusively in galaxies dominated by an old, bulge-like stellar population, regardless of the LINER/TO emission-line classification.

(ii) Diluted profiles, on the other hand, are produced by a central 'young' population (CYP) dominated by stars of 10^8–10^9 yr, whose relatively blue continuum dilutes the W_λ of metal lines with respect to their off-nuclear values.

(iii) Although concentrated in the nucleus, these CYPs are spatially extended, reaching distances of up to 400 pc from the nucleus.

(iv) The relation between diluted profiles and nuclear stellar population is clearly expressed by the ~ one-to-one relation between the radial dilution index δ_λ and the nuclear W_λ for the Ca II K line: virtually all sources with $\delta_K > 10$ per cent have $W_K^{nuc} < 15$ Å, and vice versa. This range of W_K^{nuc} corresponds exactly to our definition of 'young' stellar population, meaning populations of 1 Gyr or less.

(v) Because these stars are found almost exclusively in objects with [O I]/H$\alpha \leqslant 0.25$ (Papers I and II), it follows that stellar population gradients are typical of young-TOs. The fact that these stars are located in their central regions, and not spread over the whole galaxy, reinforces the suggestion that they are somehow connected to the ionization of the nuclear gas.

Secondly, a more detailed analysis of stellar population gradients was achieved by means of a decomposition of each spectra in terms of templates representative of very young ($\leqslant 10^7$ yr), intermediate

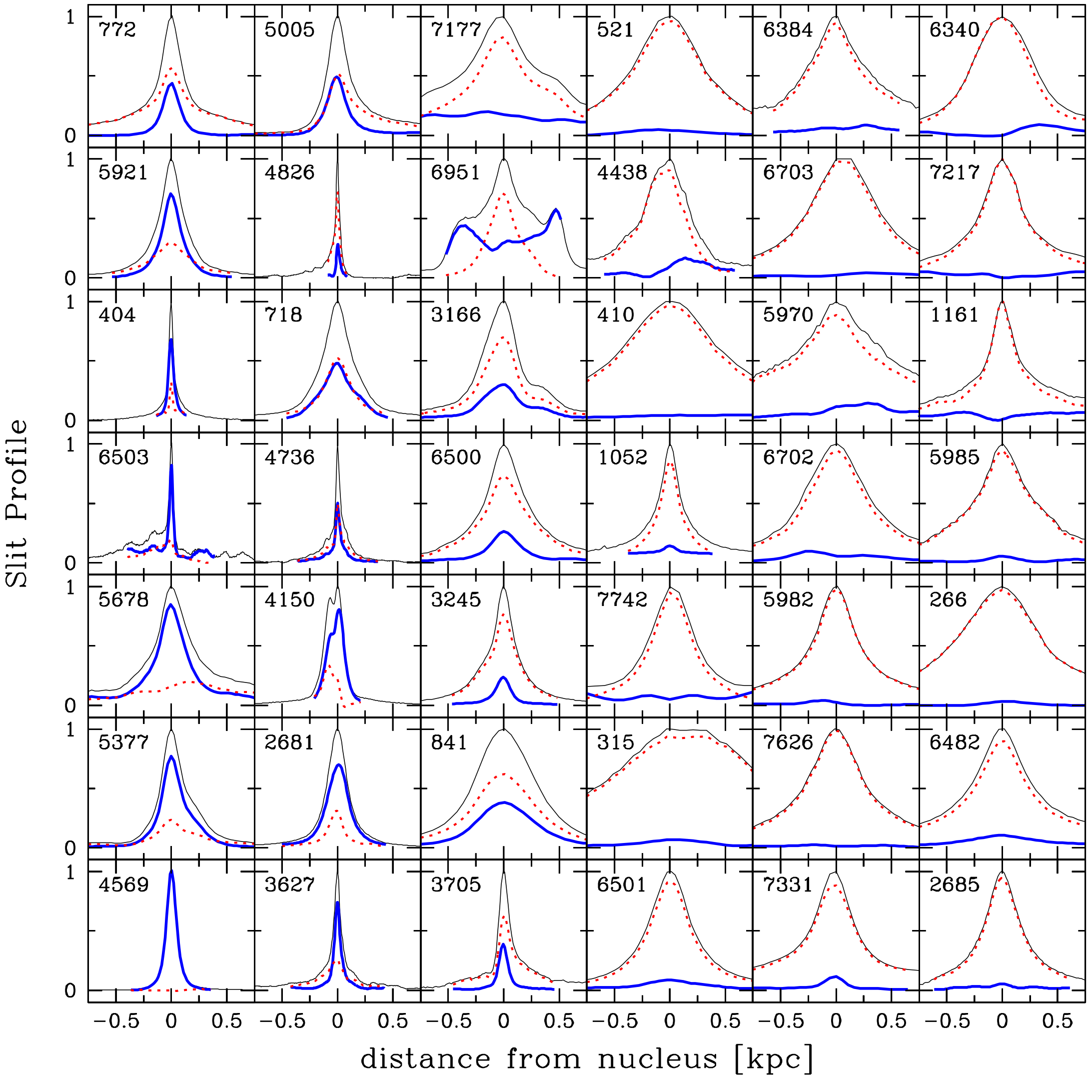

Figure 28. Normalized slit brightness profiles (thin black line), decomposed into young (thick solid blue line) and old components (dotted red). The ordering of the galaxies is as in Fig. 26.

age (10^8–10^9 yr) and old (10^{10} yr) stellar populations. This analysis shows the following.

(vi) The CYPs in young-TOs account for at least ∼1/3 of the total flux at 4020 Å. We confirm the finding of Papers I and II that these populations are dominated by 10^8–10^9 yr stars. Young starbursts, even when present, make a small contribution to the optical light.

(vii) Yet another property which distinguishes young-TOs from other members of the LLAGN family is dust content. Young-TOs are ∼ three times more extincted than old-LINERs and old-TOs. This finding is confirmed using the HFS97 measurements of the $\mathrm{H}\alpha/\mathrm{H}\beta$ ratio.

(viii) Dust tends to be concentrated towards the nucleus, although asymmetric extinction profiles are also common.

(ix) The radial flux distribution of CYPs have HWHM radii of ∼100 pc or less. While their core is at best partly resolved in our data, their outer regions are clearly resolved.

(x) The 4020-Å luminosities of the CYPs are within an order of magnitude of $10^{4.3}\ \mathrm{L}_\odot\ \text{Å}^{-1}$, implying B-band absolute magnitudes of ~ -15 and masses of the order of $\sim 10^7$–$10^8\ \mathrm{M}_\odot$. This population was 10–100 times more luminous in their formation epoch, at which time young massive stars would have completely outshone the bulge light. The active nucleus would also be swamped by these young starbursts, unless it too was brighter in the past.

This investigation has unveiled several interesting connections between stellar population, emission-line properties, spatial distribution and extinction, paving the road to a better understanding of the physics of LLAGNs. Future papers in this series will explore these and other connections in further detail.

ACKNOWLEDGMENTS

RCF and TSB acknowledge the support from CNPq, PRONEX and Instituto do Milênio. RGD acknowledges support by Spanish Ministry of Science and Technology (MCYT) through grant AYA-2001-3939-C03-01. The data presented here have been taken using the Andalucia Faint Object Spectrograph and Camera (ALFOSC), which is owned by the Instituto de Astrofísica de Andalucía (IAA) and operated at the NOT under agreement between IAA and the NBIfAFG of the Astronomical Observatory of Copenhagen. We are grateful

Table 4. CYP size and luminosity estimates from the template decomposition analysis. Columns 4 and 5 give the total and CYP monochromatic luminosities at 4020 Å integrated along the slit and extrapolated to two dimensions, in units of $L_\odot$ Å^{-1}. Numbers in parentheses are the dereddened luminosities.

NGC (1)	$R_{\rm CYP}$ (arcsec) (2)	$R_{\rm CYP}$ (pc) (3)	$\log L_{\rm tot}$ (4)	$\log L_{\rm CYP}$ (5)
0404[a]	2.5	29	3.77 (4.08)	3.54 (3.87)
0718	1.3	133	5.14 (5.17)	4.59 (4.64)
0772	0.5	79	5.06 (5.21)	4.10 (4.32)
3245	0.7	74	5.15 (5.19)	4.18 (4.22)
3367	0.4	90	5.00 (5.35)	4.91 (5.28)
3627	0.9	30	4.31 (4.60)	3.93 (4.26)
3705	0.6	48	4.24 (4.44)	3.48 (3.72)
4150	2.1	98	4.53 (5.00)	4.15 (4.70)
4569	0.6	53	5.20 (5.53)	5.19 (5.50)
4736	1.0	21	4.64 (4.77)	4.20 (4.34)
4826	0.9	19	3.89 (4.05)	3.11 (3.36)
5005	0.9	98	5.15 (5.45)	4.55 (4.93)
5377	0.7	104	5.11 (5.36)	4.85 (5.10)
5678	0.8	135	4.89 (5.53)	4.60 (5.27)
5921	0.8	95	5.03 (5.21)	4.63 (4.83)
6503	0.7	19	3.30 (3.61)	3.01 (3.33)

Note. [a]Observed under non-photometric conditions.

to the IAA director for the allocation of 5.5 nights of the ALFOSC guaranteed time. Data were also taken at KPNO, National Optical Astronomy Observatories, which are operated by the Association of Universities for Research in Astronomy (AURA), Inc., under a cooperative agreement with the National Science Foundation (NSF). The National Radio Astronomy Observatory is a facility of the NSF, operated under cooperative agreement by AURA, Inc. This research made use of the NASA/IPAC Extragalactic Database (NED), which is operated by the Jet Propulsion Laboratory, Caltech, under contract with NASA.

REFERENCES

Balogh M. L., Morris S. L., Yee H. K. C., Carlberg R. G., Ellingson E., 1999, ApJ, 527, 54
Barth A. J., Ho L. C., Filippenko A. V., Sargent W. L. W., 1998, ApJ, 96, 133
Boisson C., Joly M., Moultaka J., Pelat D., Serote Roos M., 2000, A&A, 357, 857
Bruzual G., Charlot S., 2003, MNRAS, 344, 1000
Cardelli J. A., Clayton G. C., Mathis J. S., 1989, ApJ, 345, 245
Cid Fernandes R., Storchi-Bergmann T., Schmitt H. R., 1998, MNRAS, 297, 579
Cid Fernandes R., Heckman T. M., Schmitt H. R., González Delgado R. M., Storchi-Bergmann T., 2001, ApJ, 558, 81
Cid Fernandes R. et al., 2004a, ApJ, 605, 105 (Paper I)
Cid Fernandes R., Gu Q., Melnick J., Terlevich E., Terlevich R., Kunth D., Rodrigues Lacerda R., Joguet B., 2004b, MNRAS, 355, 273
González Delgado R. M., Heckman T. M., Leitherer C., 2001, ApJ, 546, 845
González Delgado R. M., Cid Fernandes R., Pérez E., Martins L. P., Storchi-Bergmann T., Schmitt H. R., Heckman T. M., Leitherer C., 2004, ApJ, 605, 127 (Paper II)
Heckman T. M., González Delgado R. M., Leitherer C., Meurer G., Krolik J., Wilson A. S., Koratkar A., Kinney A., 1997, ApJ, 482, 114
Ho L. C., Filippenko A. V., Sargent W. L. W., 1997, ApJS, 112, 315 (HFS97)
Ho L. C., Filippenko A. V., Sargent W. L. W., 2003, ApJ, 583, 159
Joguet B., Kunth P., Melnick J., Terlevich R., Terlevich E., 2001, A&A, 380, 19
Kenney J. D. P., Yale E. E., 2002, ApJ, 567, 865
Leitherer C. et al., 1999, ApJS, 123, 3
Maoz D., Filippenko A. V., Ho L. C., Macchetto F. D., Rix H.-W., Schneider D. P., 1996, ApJS, 107, 215
Pérez E., Márquez I., Marrero I., Durret F., González Delgado R. M., Masegosa J., Maza J., Moles M., 2000, A&A, 353, 893
Raimann D., Storchi-Bergmann T., González Delgado R. M., Cid Fernandes R., Heckman T. M., Leitherer C., Schmitt H. R., 2003, MNRAS, 339, 772
Schlegel D. J., Finkbeiner D. P., Davis M., 1998, ApJ, 500, 525
Storchi-Bergmann T., Cid Fernandes R., Schmitt H. R., 1998, ApJ, 501, 94
Storchi-Bergmann T., Schmitt H. R., Cid Fernandes R., Heckman T. M., 2001, ApJ, 559, 147

This paper has been typeset from a TEX/LATEX file prepared by the author.